Multi-parametric thrombus profiling microfluidics detects intensified biomechanical thrombogenesis associated with hypertension and aging

Authors: Misbahud Din[1,2], Souvik Paul[1,2], Sana Ullah[1,2], Haoyi Yang[3], Rong-Guang Xu[1,2,4], Nurul Aisha Zainal Abidin[5], Bari Chowdhury[1,2], Fangyuan Zhou[6], Stephenie Rogers[1], Mariel Miller[1,2], Atreyee Biswas[1,2], Liang Hu[7], Zhichao Fan[8], Christopher Zahner[2], Zi Chen[4], Megan Berman[9], Lingzhou Xue[3], Lining Arnold Ju[5], Yunfeng Chen[1,2*]

Affiliations:

[1]Department of Biochemistry and Molecular Biology and [2]Department of Pathology, University of Texas Medical Branch, Galveston, Texas 77555, USA.

[3]Department of Statistics, The Pennsylvania State University, University Park, Pennsylvania 16802, USA

[4]Division of Thoracic Surgery, Brigham and Women's Hospital and Harvard Medical School, Boston, Massachusetts 02115, USA

[5]School of Biomedical Engineering, The University of Sydney, Darlington, NSW 2008, Australia

[6]Coulter Department of Biomedical Engineering, Georgia Institute of Technology, Atlanta, Georgia 30332, USA

[7]School of Integrative Medicine, Shanghai University of Traditional Chinese Medicine, Shanghai 201203, China

[8]Department of Immunology, School of Medicine, UConn Health, Farmington, Connecticut 06030, USA

[9]Department of Internal Medicine, University of Texas Medical Branch, Galveston, Texas 77555, USA

*Corresponding to: Yunfeng Chen, 224 11th ST, MRB #7.138B, Galveston, TX 77555-0645, yunfchen@utmb.edu, 409-772-0027

Abstract: Arterial thrombosis, which represents a critical complication of cardiovascular diseases, is a leading cause of death and disability worldwide with no effective bioassay for clinical prediction. As a symbolic feature of arterial thrombosis, severe stenosis in the blood vessel creates a high-shear, high-gradient flow environment that effectively facilitates platelet aggregation towards vessel occlusion even with platelet amplification loops inhibited. However, no approach is currently available to comprehensively characterize the size, composition and platelet activation status of thrombi forming under this biorheological condition. Here, we

present a thrombus profiling assay that monitors the multi-dimensional attributes of thrombi forming in conditions mimicking the physiological scenario of arterial thrombosis. Using this platform, we demonstrate that different receptor–ligand interactions contribute distinctively to the composition and activation status of the thrombus. Our investigation into hypertensive and older individuals reveals intensified biomechanical thrombogenesis and multi-dimensional thrombus profile abnormalities, demonstrating a direct contribution of mechanobiology to arterial thrombosis and endorsing the diagnostic potential of the assay. Furthermore, we identify the hyperactivity of GPIbα-integrin $\alpha_{IIb}\beta_3$ mechanosensing axis as a molecular mechanism that contributes to hypertension-associated arterial thrombosis. By studying the interactions between anti-thrombotic inhibitors and hypertension, and the inter-individual variability in personal thrombus profiles, our work reveals a critical need for personalized anti-thrombotic drug selection that accommodates each patient's pathological profile.

INTRODUCTION

Arterial thrombosis, which describes the formation of pathological blood clots in the artery, is one of the leading causes of mortality and morbidity worldwide[1,2]. Pathological conditions such as hypertension, diabetes, metabolic syndrome and aging not only exacerbate thrombotic risks but also foster resistance to conventional antiplatelets that target soluble agonist (e,g., ADP, thrombin)-induced platelet activation and aggregation[3-6], contributing to high incidence and recurrence rates of cardiovascular diseases (CVD)[7]. However, the associated mechanisms are not fully elucidated. The current clinical paradigm is further challenged by the lack of a standard bioassay for evaluating thrombotic risks[8,9].

As an understudied but symbolic mechanism of arterial thrombosis, platelets can be mechanically driven by the elevated shear stress and shear gradient caused by vessel stenosis to form large aggregates[5,10]—a phenomenon we termed “biomechanical platelet aggregation”[11,12]. Biomechanical platelet aggregation is primarily contributed by discoid platelets, wherein shear-induced VWF activation[13] and GPIbα–VWF catch bond[14] enable the initial aggregation of platelets in an activation-independent manner; then, the GPIbα–VWF binding under force initiates GPIbα mechanosignaling that leads to integrin $\alpha_{IIb}\beta_3$ activation to an intermediate affinity and an extended-close ($E^+Act.^-$) conformation[12], which binds to Fg and VWF and allows

more stable thrombus development. Notably, $E^{+}Act.^{-}$ integrin $\alpha_{IIb}\beta_3$ is only achievable via GPIbα mechanosignaling but not soluble agonist-induced platelet activation[12]. biomechanical platelet aggregation cannot be effectively inhibited by conventional antiplatelets or amplification loop blockers (ALBs), but is strongly impeded by shear rate decrease and is reversible upon the release of vessel stenosis, underscoring a primary role of platelet mechanosensing[10,12]. However, while the mechanobiology of platelets is already barely investigated in pathological contexts[15,16], whether biomechanical platelet aggregation can be intensified by any thrombotic risk factor, thereby directly contributing to higher incidence of CVD in certain human populations was never studied. Also, existing methods for observing biomechanical platelet aggregation[10,12,17] cannot provide all-around information and quantitative analysis regarding the composition of the thrombus or the platelet activation status within, which hinders our understanding of arterial thrombosis and improvement of anti-thrombotic treatment. For example, platelets in biomechanical platelet aggregation are crosslinked via three molecular interactions: glycoprotein (GP) Ibα–von Willebrand factor (VWF), integrin $\alpha_{IIb}\beta_3$–VWF and integrin $\alpha_{IIb}\beta_3$–fibrinogen (Fg)[10,12,18]. How they respectively mediate the VWF and Fg levels and platelet activation in the biomechanical thrombus, and whether they are dysregulated by thrombotic risk factors to cause abnormalities in biomechanical thrombogenesis remain unclear.

To address these outstanding clinical and scientific needs, we developed a thrombus profiling assay that combines a standard stenosis microfluidics setup with multi-color thrombus staining. It enables quick and all-around thrombus characterization under conditions that mimic biorheological settings of arterial thrombosis. Using this assay, we delineated the differential roles of complex platelet crosslinking mechanisms in biomechanical thrombogenesis. We identified exacerbated biomechanical thrombogenesis and multi-dimensional thrombus abnormality associated with hypertension and aging, unravelling a clinical linkage between mechanobiology and arterial thrombosis. With complementary data from four other experimental approaches, we further demonstrated that GPIbα and integrin $\alpha_{IIb}\beta_3$ receptors on hypertension patients' platelets have endogenous hyperactivity, thereby unravelling the molecular mechanisms underlying platelet mechanobiological dysfunction in hypertension-associated arterial thrombosis. By using the thrombus profiling assay to study drug-disease interactions and acquire personal thrombus profiles, we identified a gap in standard approaches of anti-thrombotics evaluation, which urges a re-evaluation of the efficacy and safety of anti-thrombotics using the

'thrombus profile' and in the context of different pathology models. All above results also showcase the potential of our thrombus profiling assay for anti-thrombotic drug screening, diagnosis of thrombotic risks, and personalized anti-thrombotic regimen selection.

RESULTS

Thrombus profiling assay: development and validation

Our microfluidic chip is composed of 10 rectangular (200×50 μm^2) channels with respective inlets and outlets for tubing connection (Fig. 1a,b). A pump drives a syringe to perfuse blood (0.5 mL) through the channel. An 80% stenosis site stimulates biomechanical thrombogenesis (Fig. 1c). A perfusion rate of 18 $\mu L\ min^{-1}$ was selected, which creates a wall shear stress (WSS) of 860 dyn cm^{-2} at the stenosis site according to fluid dynamics simulation (Fig. 1d; Supp. Fig. 1a,f). The same stenosis site WSS is achieved by an inlet wall shear rate of 1489 s^{-1} in a circular vessel with the same cross-sectional area (Supp. Fig. 1b,d,f), mimicking human arterioles[19], human arteries during systole, and mouse arteries[20]. With the above settings, platelet thrombi can be consistently observed within the channel, which is primarily driven by shear force because no external agonist is added to the blood and the high-speed perfusion prevents the localized accumulation of agonists released from attached platelets and red blood cells. Due to the high shear force, most thrombi have a tendency of growing towards the downstream side of the stenosis. Nonetheless, most thrombi (>85%) cover the whole stenosis apex, and most (>85%) thrombi have the point in their contour most close to the opposing channel wall positioned above the stenosis apex (Supp. Fig. 2), making the stenosis apex still the most vulnerable position for occlusion.

To comprehensively characterize the thrombus, 7 biomarkers with their respective molecular sensors were selected (Fig. 1e). Platelets are reported by SZ22, a monoclonal antibody (mAb) against integrin $\alpha_{IIb}\beta_3$[12]. Fg is reported by purified Fg that spikes the blood at 1% of plasma concentration. VWF is reported by non-inhibitory mAb 2.2.9[21]. P-selectin is reported by AK4 to signify platelet α-granule release[22]. Phosphatidylserine (PS) exposure in the membrane is reported by Annexin V to signify platelet procoagulant function[23]. Conformationally extended (E^+) and fully activated (Act.) integrin $\alpha_{IIb}\beta_3$ are detected by mAbs MBC370.2 and PAC-1, respectively, which together report the integrin activation status[12]. The above sensors were

grouped into 2 sets for fluorophore conjugation (Fig. 1e), where SZ22 appears in both sets for reference. All sensors have negligible influence on thrombogenesis (Supp. Fig. 3).

Fluorescent signals were observed from all 7 biomarkers (Fig. 1f). Agreeing with previous observations[10,24], real-time tracking showed rapid thrombogenesis in the first 300-400 s followed by a quasi-steady phase, in which the thrombus reaches a relative equilibrium between platelet aggregation and disaggregation (Fig. 1g). Thus, we selected 450 s after the onset as the time point for quantitating fluorescent signals so as to assess the thrombus in the fully developed status while avoid long observation time which would require a greater volume of blood, increase the test cost, and lower the test throughput (Fig. 1h). Signal intensities of Fg, VWF, P-selectin, PS and E^+ and Act. $\alpha_{IIb}\beta_3$ were normalized by platelet signal to assess their enrichment (Fig. 1i), where the high E^+ $\alpha_{IIb}\beta_3$ signal and low Act. $\alpha_{IIb}\beta_3$ signal agree with our previous discovery that biomechanical platelet aggregation is mainly mediated by an intermediate activation state of $\alpha_{IIb}\beta_3$ integrins[12]. P-selectin expression and low-level PS exposure observed here (Fig. 1f,i; further confirmed using different microscope setup, staining agents and microfluidic channel design (Supp. Fig. 4)) should be induced by GPIbα and/or integrin $\alpha_{IIb}\beta_3$ mechanosignaling[25-29]. The total signal intensity of platelets (1st dimension, indicating thrombus size) and the normalized signal intensities of Fg, VWF, P-selectin, PS and E^+ and Act. $\alpha_{IIb}\beta_3$ (2nd-7th dimensions) are summarized into a 7-dimension thrombus profile (Fig. 1f,i).

Blood stored for >6 h or refrigerated overnight both failed to generate visible thrombi (Fig. 1h), which is likely due to a loss of platelet activity during room temperature storage and GPIbα shedding during cold storage[30], respectively. Activated platelets can release and/or help produce soluble agonists such as thromboxane A2, ADP, and thrombin to further activate themselves and recruit surrounding platelets to the growing thrombus, wherein the activation signaling processes are called amplification loops. However, conventional antiplatelets aspirin (targeting thromboxane A2 (TXA2)) and clopidogrel (targeting $P2Y_{12}$–ADP interaction) rendered negligible inhibition to the biomechanical thrombogenesis both separately and combined at twice or 20 times of human plasmatic concentrations[31] (Fig. 1j). In contrast, both drugs were demonstrated to significantly inhibit ADP or collagen-induced platelet aggregation at much lower concentrations[31]. Also, a platelet ALB cocktail (including apyrase, MRS2179 and 2-MeSAMP to block ADP, indomethacin to block TXA2, and hirudin to block thrombin, all at

saturating concentrations) only reduced the thrombus size by ~20% (Fig. 1j). These results corroborate the previous observations that inhibiting platelet amplification loops is ineffective in inhibiting biomechanical platelet aggregation[10,12,32], demonstrating a secondary role of soluble agonists in biomechanical thrombogenesis.

Delineating the contribution of different receptor–ligand interactions

Biomechanical platelet aggregation is mainly mediated by a mechanosensing axis on the platelet surface composed of two mechanoreceptors: GPIbα and integrin $\alpha_{IIb}\beta_3$. GPIbα first binds to VWF to initiate platelet crosslinking, during which GPIbα mechanosignaling induces integrin $\alpha_{IIb}\beta_3$ intermediate activation ($E^+Act.^-$). The activated integrin $\alpha_{IIb}\beta_3$ binds to its ligands VWF and Fg to reinforce the platelet crosslinking process and also trigger its own further activation towards the fully activated state ($E^+Act.^+$)[12]. To investigate how the above platelet-crosslinking mechanisms, namely, GPIbα–VWF, integrin $\alpha_{IIb}\beta_3$–VWF, and integrin $\alpha_{IIb}\beta_3$–Fg interactions, respectively mediate the growth, composition and activation status of biomechanical thrombi, blood was treated with a panel of highly specific inhibitory mAbs to inhibit them one at a time (Fig. 2a). AK2 and NMC4 both inhibit GPIbα–VWF interaction, with AK2 targeting GPIbα, and NMC4, previously shown to have anti-thrombotic effects[33], targeting VWF A1 domain (VWFA1) which binds to GPIbα[33,34]. LJ-P5 and 152B6 both inhibit integrin $\alpha_{IIb}\beta_3$–VWF interaction, with LJ-P5 blocking integrin $\alpha_{IIb}\beta_3$ binding to VWF but not Fg[35], and 152B6 blocking VWF binding to integrin $\alpha_{IIb}\beta_3$ but not GPIbα[36]. 7E9, LJ-155B39 and LJ-134B29 inhibit integrin $\alpha_{IIb}\beta_3$–Fg interaction by respectively blocking one of the three integrin-binding sites in Fg: γ408-411 (AGDV), Aα95-98 (RGDF) and Aα572-575 (RGDS)[37,38].

Single fluorescence imaging was first used to measure the dose-dependency of the above mAbs in inhibiting thrombogenesis (Fig. 2b-e). Only AK2 and NMC4, but not the other mAbs, eliminated thrombogenesis (Fig. 2c-e), underscoring GPIbα–VWF interaction as the initiator of biomechanical platelet aggregation[10,12]. At high concentrations, both LJ-P5 and 152B6 reduced the thrombus size to <20% (Fig. 2d), and the cocktail of 7E9, LJ-155B39 and LJ-134B29 also reduced the thrombus size to ~5% (Fig. 2e), indicating an important role of both integrin $\alpha_{IIb}\beta_3$–VWF and $\alpha_{IIb}\beta_3$–Fg interactions. When added alone, 7E9 achieved a strong inhibitory effect comparable to the cocktail, highlighting the primary role of AGDV in Fg for integrin $\alpha_{IIb}\beta_3$

binding[39,40]. However, LJ-155B39 and LJ-134B29 also manifested considerable inhibition, unraveling underestimated contributions of the RGD sequences[41] to arterial thrombosis (Fig. 2e).

Half-maximal inhibitory concentrations (IC50) were acquired for these mAbs via model fitting (Supp. Table 1), which were then used in thrombus profiling. Both AK2 and NMC4 significantly decreased VWF, P-selectin, and E^+ and Act. $\alpha_{IIb}\beta_3$ levels in the thrombus (Fig. 2f,g). In comparison, LJ-P5 and 152B6 only reduced VWF enrichment, while 7E9, LJ-155B39, and LJ-134B29 only reduced Fg enrichment; neither set of mAbs inhibited PS exposure, P-selectin expression, or integrin $\alpha_{IIb}\beta_3$ activation (Fig. 2h-l). None of the above mAbs affected the average signal intensity of SZ22-FITC, ruling out the possibility that the reduced VWF and Fg signals were due to increased platelet density (Supp. Fig. 5a). Altogether, our results indicate that different platelet-crosslinking mechanisms cooperatively mediate biomechanical thrombogenesis, with each having a distinct focus in their contribution to the thrombus composition and activation status.

To succinctly express the effects of different factors on biomechanical platelet aggregation, we created an "effect barcode" system with 7 columns each corresponding to one dimension of the thrombus profile. A positive, neutral, or negative effect of a factor on a dimension is respectively represented by a bar at the top, middle or bottom of the column, also numerically expressed as '+', '0', or '-'. Using this system, the effects of AK2 and NMC4 on the thrombus profile are both summarized as [- 0 - - 0 - -], those of LJ-P5 and 152B6 as [- 0 - 0 0 0 0], and those of 7E9, LJ-155B39 and LJ-134B29 as [- - 0 0 0 0 0] (Fig. 2m).

Identifying an 'addition rule' in the effect barcode system

Intrigued by how different receptor–ligand interactions synergize in mediating biomechanical thrombogenesis, we tested inhibitors with combinational effects. 7E3 (prototype of the antiplatelet abciximab) and 10E5 are mAbs that block integrin $\alpha_{IIb}\beta_3$ binding to both Fg and VWF[12,42,43]. Unlike inhibitors of integrin $\alpha_{IIb}\beta_3$–VWF or $\alpha_{IIb}\beta_3$–Fg, both 7E3 and 10E5 eliminated thrombogenesis at high concentrations (Fig. 3a). At IC50, both mAbs reduced Fg and VWF levels in the thrombus without affecting platelet activation markers, rendering an effect barcode of [- - - 0 0 0 0]. Interestingly, this barcode equals the add-up of those of integrin $\alpha_{IIb}\beta_3$–VWF ([- 0 - 0 0 0 0]) and $\alpha_{IIb}\beta_3$–Fg ([- - 0 0 0 0 0]) inhibitors.

Negatively charged nanoparticles inhibit platelet aggregation at high shear rates due to their inhibition of VWF extension and, therefore, VWF–platelet interactions[44]. We tested two sizes of polystyrene negatively charged nanoparticles (PS-CNP) (50 and 510 nm), both showing biphasic dose-dependency in thrombus inhibition, consistent with the original report[44]. A concentration that decreases the thrombus size by ~50% was estimated for the 510 nm PS-CNP to perform thrombus profiling (Fig. 3e), which derived an effect barcode of [- 0 - - 0 - -] (Fig. 3f). Again, this barcode equals the add-up of those of GPIbα–VWF ([- 0 - - 0 - -]) and integrin $\alpha_{IIb}\beta_3$–VWF ([- 0 - 0 0 0 0]) inhibitors. The above results demonstrate that the mathematical addition rule applies to the effect barcode system.

Multi-dimensional thrombus profile abnormality in hypertension and aging

Aging and hypertension are two well-known strong risk factors for thrombosis[45,46]. To test the performance of our assay in identifying risks of arterial thrombosis, we first compared the thrombus size of healthy adults at different ages and identified that older ages (≥50) significantly increase the thrombus size (Fig. 4a). Furthermore, we tested blood samples from primary hypertension patients (Supp. Table 3), which formed much larger biomechanical thrombi than healthy young subjects (Fig. 4b). By fitting the "thrombus size versus time" curves with the sigmoidal model, it was observed that unlike the growth of healthy young subjects' thrombi which approached a plateau at ~400 s, hypertension patients' thrombi remained in the rapid development phase until ~500 s, also indicating a clear prothrombotic tendency (Fig. 4b). Characterizing the thrombus profile revealed that aging and hypertension, either alone or together, significantly increased the thrombus size, Fg level as well as integrin $\alpha_{IIb}\beta_3$ activation in the thrombi, rendering the same effect barcode of [+ + 0 0 0 + +] (Fig. 4c). Two-way ANOVA with variance heterogeneity further identified a significant interaction between hypertension and aging in increasing the thrombus size, indicating a synergy effect between the two factors (Fig. 4d). None of the above abnormalities was contributed by platelet density changes in the thrombus or hematocrit changes or platelet count increase in the blood (Supp. Fig. 5b-e).

Considering the scattering pattern of the signal intensity of the different biomarkers (Fig. 4c), which is likely due to inter-individual variability, we performed multiple statistical analyses to evaluate their inter-correlation and their performance in distinguishing different cohorts.

Firstly, by using linear regression model, Spearman rank correlation coefficient[47] and Kendall's tau correlation coefficient[48], a positive correlation was consistently identified between thrombus size and Fg, E^+ $\alpha_{IIb}\beta_3$ and Act. $\alpha_{IIb}\beta_3$ levels (Fig. 4e, Supp. Fig. 6), with E^+ $\alpha_{IIb}\beta_3$ being the strongest correlating factor as judged by the linear fitting slope (Supp. Table 2). Secondly, among all markers, E^+ $\alpha_{IIb}\beta_3$ has the best performance in separating healthy young from hypertensive and/or older age groups (Fig. 4e, Supp. Fig. 6a-e), with specificity and sensitivity respectively reaching 84% and 85%, comparable to the performance of thrombus size (Supp. Table 2). The consistency of E^+ $\alpha_{IIb}\beta_3$ level with thrombus size in group separation also reached 78%. Altogether, these results unraveled intensified biomechanical thrombogenesis and multi-dimensional thrombus profile abnormality associated with hypertension and aging, and suggest E^+ $\alpha_{IIb}\beta_3$ as a potential biomarker for intensified biomechanical thrombogenesis.

Next, we investigated how the healthy condition of the hypertension patients affect their thrombus profiles. Firstly, neither thrombus size nor E^+ $\alpha_{IIb}\beta_3$ level was correlated with the disease duration, systolic or diastolic blood pressure, or the sum of the two in both young and older patients (Fig. 4f, Supp. Fig. 7). Secondly, because type 2 diabetes, obesity and dyslipidemia are also risk factors of CVD, we assessed the relationship of the patients' thrombus size and E^+ $\alpha_{IIb}\beta_3$ level with their hemoglobin A1C (HbA1C) level, body mass index (BMI), and total cholesterol, low-density lipoprotein cholesterol (LDL-C), high-density lipoprotein cholesterol (HDL-C) and triglyceride levels. However, again, no significant correlation was identified (Fig. 4f, Supp. Fig. 7). Notably, most patients enrolled in this study had hypertension well controlled by medication (systolic/diastolic blood pressure <140/90 mmHg, respectively) and were absent of comorbidities (Fig. 4f; Supp. Table 3). Thus, our results indicate that hypertension can independently cause intensified biomechanical thrombogenesis and thrombus profile abnormality even with relatively short disease duration and effective antihypertensive medication. Nonetheless, we cannot exclude the likelihood that poorly controlled blood pressure and/or comorbidities can have extra contributions to the thrombus profile abnormality.

Lastly, we inspected whether demographics other than age affect the thrombus profile. Within healthy young as well as hypertensive and/or older subjects, no significant difference in the thrombus size or E^+ $\alpha_{IIb}\beta_3$ level was found between males and females or among different races/ethnicities (Fig. 4g-l). Seemingly in discrepancy with previous reports of a higher

prevalence of CVD in males than in females and slight prevalence differences in different ancestries, these results corroborates more careful cohort studies demonstrating that the correlation of gender and ancestry with thrombotic risks is mainly due to the differential prevalence of social determinants of health and cardiovascular risk factors[46,49,50].

Hypertension causes hyperactivity of GPIbα-integrin $\alpha_{IIb}\beta_3$ mechanosensing axis

We previous identified that the intermediate activation state of $\alpha_{IIb}\beta_3$ integrin with an extended-close conformation ($E^+Act.^-$) plays a crucial role in biomechanical platelet aggregation[12]. Thus, the over-expressed E^+ $\alpha_{IIb}\beta_3$, predominantly $E^+Act.^-$ $\alpha_{IIb}\beta_3$ (Supp. Fig. 6f) in the thrombi of hypertensive patients should directly contribute to the intensified biomechanical thrombogenesis. We hypothesize that the E^+ $\alpha_{IIb}\beta_3$ over-expression is likely due to 1) hyperactivity in GPIbα, with triggers stronger mechanosignaling for integrin activation[12], and/or 2) integrin $\alpha_{IIb}\beta_3$ pre-activation in the patients' body. To test these two hypotheses, we used four complementary approaches to investigate the activities of GPIbα and integrin $\alpha_{IIb}\beta_3$ in hypertension patients.

Firstly, conventional laminar flow chamber assay was used to measure the overall ligand binding activity of the two receptors. Unlike the stenosis assay, here the channels adopt a plain surface pre-coated with VWFA1 or Fg to engage GPIbα and integrin $\alpha_{IIb}\beta_3$, respectively. Plasma in the blood was depleted and replaced with buffer to prevent the interference of endogenous VWF and Fg and avoid platelet aggregation. By perfusing blood through the channels under varied shear rates, it was shown that platelets from hypertensive young, hypertensive older and healthy older subjects all achieved much higher surface coverage and slower rolling on VWFA1 than healthy young group (Fig. 5a-c, Supp. Fig. 8a,b). On the other hand, only hypertensive young and hypertensive older groups achieved high surface coverage on Fg, while healthy young and healthy older groups were low (Fig. 5a,d). These results indicate that both hypertension and aging cause GPIbα hyperactivity, but only hypertension induces hyperactivity in integrin $\alpha_{IIb}\beta_3$ at the same time. The activities of GPIbα and integrin $\alpha_{IIb}\beta_3$ on hypertensive young and hypertensive older subjects' platelets were comparable, suggesting an absence of synergistic effect from aging (Fig. 5b-d). Therefore, for all mechanistic studies below, we did not view results from hypertensive young and hypertensive older subjects separately.

Secondly, a single-molecule force spectroscopy technique, biomembrane force probe (BFP)[51], was used to measure the ligand binding of single platelets. A micropipette-aspirated biotinylated human red blood cell (RBC) was used as an ultrasensitive force transducer, and a probe bead co-functionalized with streptavidin and VWFA1 or Fg was glued to the RBC apex. A platelet was aspirated by an opposing micropipette and driven to repeatedly contact the bead, which induced adhesion events to measure the receptor–ligand binding kinetics (Fig. 5e). Adhesion frequency assay was first deployed to enumerate the absence or presence of adhesion events after long contacts to calculate the steady-state adhesion frequency, P_a[52]. The P_a of hypertensive subjects' platelets adhering to the same batch of VWFA1 and Fg beads were significantly higher than healthy young (Fig. 5f,i), reflecting a significantly higher effective avidity (ligand-binding capability of each unit of platelet surface area) of both GPIbα and integrin $\alpha_{IIb}\beta_3$ (Fig. 5g,j, *left*), which is consistent with the platelets' enhanced capability of engaging VWFA1 and Fg in the flow chamber (Fig. 5a-d). Dividing effective avidities by the receptors' surface density showed that the average effective affinity of GPIbα and integrin $\alpha_{IIb}\beta_3$ on the hypertensive subjects' platelets were also significantly enhanced (Fig. 5g,j, *right*). Then, the BFP force-clamp assay was used to measure the stability of single GPIbα–VWFA1 and integrin $\alpha_{IIb}\beta_3$–Fg bonds under force. This was achieved by adjusting the contact time between the bead and the platelet to achieve $P_a \approx 20\%$, thereby realizing a ~90% probability of single bonds[52]. The GPIbα–VWFA1 bond lifetime of hypertensive subjects' platelets manifested a 'slip bond' instead of a triphasic 'slip-catch-slip' trend seen on healthy young subjects' platelets[53] (Fig. 5h). This resulted in a substantial prolongation of bond lifetimes under forces <20 pN (Fig. 5h). On the other hand, hypertension caused a substantial rightward and upward shift of the integrin $\alpha_{IIb}\beta_3$–Fg catch bond[12], so that the peak force increased from ~15 to ~35 pN, the peak lifetime increased from ~5 to ~10 s, and the force range where lifetime events were observable was widened from 0-40 to 0-65 pN (Fig. 5k). Notably, this lifetime curve from hypertensive subjects' platelets also resembles healthy young subjects' $E^+Act.^-$ integrin $\alpha_{IIb}\beta_3$–Fg lifetime curve characterized previously[12]. Altogether, our BFP results indicate that hypertension increases not only the avidity, but also the affinity and force-regulated ligand binding strength of GPIbα and integrin $\alpha_{IIb}\beta_3$.

Thirdly, we combined fluorescence imaging with BFP (fBFP) to study whether the increased affinity and ligand binding strength of GPIbα in hypertension patients can result in stronger

mechanosignaling to better induce integrin $\alpha_{IIb}\beta_3$ activation. Platelets pre-loaded with Ca^{2+} dye (Fura-2) were repeated stimulated by a VWFA1-coated bead in force-clamp cycles at a fixed 2-s contact time for 5 min (Fig. 5l), while the normalized intraplatelet Ca^{2+} level was monitored (Fig. 5m). Agreeing with our hypothesis, hypertension patients' platelets fluxed stronger Ca^{2+} signals—reflected by higher Ca^{2+} peak increase—than healthy young subjects' platelets under a wide force range (Fig. 5n). Unlike healthy young subjects' platelets where the Ca^{2+} signal first increases and then decreases with clamping force, mirroring their lifetime's 'catch-slip' trend, the Ca^{2+} signal of hypertension patients' platelets manifested a gradual decline with clamping force, also consistent with the shape of their GPIbα–VWFA1 lifetime slip bond (Fig. 5n). This corroborates our previous finding that the intensity of GPIbα mechanosignaling, manifested by both Ca^{2+} signaling and integrin $\alpha_{IIb}\beta_3$ activation, heavily relies on the duration of force pulling on GPIbα[54].

Fourthly, flow cytometry was used to investigate whether the $\alpha_{IIb}\beta_3$ integrins on hypertension patients' platelets are pre-activated. While similarly high expression of integrin $\alpha_{IIb}\beta_3$ and baseline expression of Act. $\alpha_{IIb}\beta_3$ and P-selectin were detected on the platelets of healthy young and hypertensive subjects, the expression of E^+ $\alpha_{IIb}\beta_3$ in the hypertensive group was found to be much higher than in the healthy young group (Fig. 5o-s). Although hypertension patients' platelets are slightly larger than healthy young subjects', a positive correlation between E^+ $\alpha_{IIb}\beta_3$ signal and platelet volume was found only in the hypertensive group but not healthy young group (Supp. Fig. 8c,d). These results indicate that hypertension patients' platelets are pre-activated, with integrin $\alpha_{IIb}\beta_3$ up-regulated to the intermediate activation state ($E^+Act.^-$) and minimal P-selectin expression.

Altogether, our results indicate that two mechanisms work in parallel to induce E^+ $\alpha_{IIb}\beta_3$ over-expression in the biomechanical thrombi of hypertensive patients (Fig. 5t): 1) some $\alpha_{IIb}\beta_3$ integrins already adopt an endogenous E^+ status rather than remaining inactive as on healthy platelets; and 2) hyperactive GPIbα triggers stronger mechanosignaling upon VWF binding, inducing more $\alpha_{IIb}\beta_3$ integrins to undergo E^+ activation than on healthy platelets.

Expanding the addition rule to drug-disease interactions

Using the thrombus profiling assay, we tested how anti-thrombotic inhibitors affect the thrombus profile of hypertension patients. Consistent with our results on healthy subjects, the combination of aspirin and clopidogrel at twice of human plasmatic concentrations[31] showed no effect on hypertension patients' thrombi (Fig. 6a). In contrasts, at IC50, NMC4 reduced the thrombus size and E^+ and Act. $\alpha_{IIb}\beta_3$ expression to healthy levels, but also lowered VWF and P-selectin levels unaffected by hypertension (Fig. 6a). The resulting effect barcode, [0 + - - 0 0 0], equals the add-up of those of NMC4 and hypertension (Fig. 6b). Similarly, adding 7E3 to hypertension patients' blood resulted in an effect barcode of [0 0 - 0 0 + +], equaling the add-up of the effect barcodes of 7E3 and hypertension (Fig. 6a,b). These results indicate that the addition rule of the barcode system can also be applied to predict drug-disease interactions. Neither NMC4 nor 7E3 completely corrected the effect barcode of hypertension, with 7E3 even incapable of suppressing the integrin $\alpha_{IIb}\beta_3$ over-activation, implying a treatment mismatch between the inhibitors and the patients.

Inter-individual variability in personal thrombus barcodes

Lastly, to evaluate the normality and abnormalities of individuals' thrombus profiles, we created the concept of "personal thrombus barcodes". From the thrombus profiles of healthy young subjects, values of each dimension were fitted to a Gaussian distribution, of which the mean±2s.d. (~95% confidence interval) was defined as the reference range ('0') (Supp. Fig. 9), and values lower or higher were defined as abnormally low ('-') and high ('+'), respectively.

Applying this system to healthy young subjects rendered all dimensions of thrombus profiles being dominated by normal values, with only very small fractions being abnormally low or high, which is consistent with the definition of the reference ranges (Fig. 6c). In contrast, much larger proportions of healthy older, hypertensive young, and hypertensive older subjects had large thrombi and high E^+ and Act. $\alpha_{IIb}\beta_3$ levels, with the fraction having high Fg levels also moderately higher (Fig. 6c). Most of these subjects (23/32) have high values in thrombus size and E^+ $\alpha_{IIb}\beta_3$ level, yet 3 subjects with abnormally large thrombi have a normal E^+ $\alpha_{IIb}\beta_3$ level. A high Act. $\alpha_{IIb}\beta_3$ level was observed in half of the subjects with large thrombi (12/26), but also in 2 subjects with normal thrombi (Supp. Fig. 10). Most subjects in these three groups (19/32) have abnormal VWF, P-selectin and PS levels, which may or may not co-exist with high values of thrombus size and E^+ $\alpha_{IIb}\beta_3$ level. Of all the 65 subjects, a total of 30 different personal thrombus

barcodes were identified (Supp. Fig. 10). Overall, the above results indicate strong inter-individual variability in the personal thrombus barcode that cannot be ascribed to disease and aging, and demonstrate obvious decoupling of the different dimensions in the thrombus profile. Notably, we repeated our test on 14 randomly picked subjects after different time intervals (from 2 weeks to 9 months). Among a total of 21 re-tests, only 2 showed changes in the personal thrombus barcodes, which were associated with the longest time intervals (7 and 9 months, respectively) (Supp. Fig. 10). This reflects high reliability of our assay and indicates that the personal thrombus profiles of individuals are relatively stable but can still vary over time.

Inter-individual variability was also observed in the subjects' responses to anti-thrombotic inhibitors. While NMC4 effectively corrected the size and E^+ $\alpha_{IIb}\beta_3$ level in most hypertension patients' thrombi, it did not uniformly modify all their personal thrombus barcodes, but instead produced three different barcodes: [0 0 0 0 0 0 0], [0 0 - 0 0 0 0], and [0 0 0 0 0 + 0] (Fig. 6c,d). Similar diversification was also found in 7E3, despite its consistent negative effect on the thrombus size and neutral effect on E^+ $\alpha_{IIb}\beta_3$ level (Fig. 6c,d). These diversifications cannot be completely ascribed to differences in the patients' original personal thrombus barcodes (Fig. 6d).

DISCUSSION

The methodology framework developed in this study for evaluating arterial thrombosis includes not only the experimental setup itself, but also the 'thrombus profile', the barcode systems, and the 'addition rule' as conceptual elements. Unlike conventional laboratory and point-of-care assays, our thrombus profiling assay mainly assesses biomechanical platelet aggregation. Because the high-shear, high-gradient blood flow associated with arterial thrombosis reinforces biomechanical platelet aggregation[10,32] and at the same time impede soluble agonist-induced platelet aggregation and coagulation by limiting local accumulation of soluble substances[55], biomechanical platelet aggregation should be one, and possibly the most, essential mechanism of arterial thrombosis. This rationalizes the outstanding performance of our thrombus profiling assay in testing clinical subjects associated with higher risks of arterial thrombosis, demonstrating its potential to clinically assess thrombotic risks in general populations. In this context, the detection of integrin $\alpha_{IIb}\beta_3$ over-activation and the identification of "treatment mismatch" using the barcode system further showcase the assay's ability in identifying the

mechanisms of prothrombotic tendency in human and in evaluating the function of anti-thrombotic drugs and candidates. Meanwhile, cost-effectiveness and low sample volume represent additional advantages. Also, with a multi-channel syringe rack and either a programmable motorized stage or a multi-camera array to observe multiple channels in parallel, the assay can reach a considerable throughput, allowing the test of ~50 samples per day. On the other hand, the assay also has the potential of evaluating bleeding tendency in patients and the bleeding side effect in antithrombotic agents[24], which warrants future investigation. As a limitation, the current judgement system for deciding normal versus abnormal thrombus barcodes is still premature, which can benefit from more detailed segmentation (e.g., borderline, stage-I, and stage-II abnormal). The assay shall also be combined with other existing diagnostic approaches, e.g., risk score assessment that is being widely used in preventive cardiology[56,57], to provide more accurate evaluation and treatment suggestions. Another limitation of our assay is that it cannot recapitulate the biomechanical scenarios of thrombosis in all different arteries and arterioles, especially in large arteries where the Reynolds number can be sufficiently high to trigger turbulence[58]. Instead, the assay shall be regarded as a tool to gauge the general shear-driven platelet "aggregatability" in blood samples.

Using a panel of mAbs with highly specific targets, we showed that all the three receptor–ligand interactions studied in this work: GPIbα–VWF, integrin $\alpha_{IIb}\beta_3$–VWF and integrin $\alpha_{IIb}\beta_3$–Fg, contribute to the size growth of biomechanical thrombi. However, GPIbα mechanosignaling appears to be more critical than integrin $\alpha_{IIb}\beta_3$ mechanosignaling to platelet activation during biomechanical thrombogenesis, as manifested by integrin $\alpha_{IIb}\beta_3$ activation and P-selectin expression. This agrees with our previous observation that GPIbα mechanosignaling serves as the initiator in the GPIbα-integrin $\alpha_{IIb}\beta_3$ mechanosensing axis, without which integrin $\alpha_{IIb}\beta_3$ cannot activate itself by binding to its own ligands[12]. We showed that GPIbα–VWF and integrin $\alpha_{IIb}\beta_3$–VWF interactions both modulate the deposition of VWF into the thrombus, while integrin $\alpha_{IIb}\beta_3$–Fg only modulates that of Fg, which seem intuitive because both VWF and Fg need to be bound to their respective platelet receptors to maintain their presence in the thrombus. However, the fact that inhibiting either VWF or Fg binding to integrin $\alpha_{IIb}\beta_3$ does not enrich the other ligand, but both reduce the thrombus size, suggests that VWF and Fg cooperate, rather than mutually compensate, in integrin $\alpha_{IIb}\beta_3$ crosslinking for biomechanical platelet aggregation. On the other hand, as shown in previous works, as the shear rate increases, the dependency of shear-

induced platelet aggregation on GPIbα activity becomes progressively stronger and on integrin $\alpha_{IIb}\beta_3$ activity progressively weaker[59]. It will be interesting to test whether changing the shear rate in our assay affects how the three receptor–ligand interactions contribute to the thrombus profile. Interestingly, our results appear to indicate that the effect barcode of each anti-thrombotic agent is dictated by its target rather than its pharmacological design. This principle may enable us to use the effect barcode to quickly narrow down the possible target(s) of uncharacterized anti-thrombotic agents. To serve the above purpose, inhibitors of other contributing factors of biomechanical platelet aggregation, e.g., mechanosignaling of GPIbα, integrin $\alpha_{IIb}\beta_3$ and Piezo1[16,60,61], all be tested to acquire their effect barcodes.

Hypertension is the leading cause of CVD and is also closely associated with antiplatelet (e.g., aspirin and clopidogrel) resistance[3,4]. Abnormal platelet activation is indicated as a major feature in the prothrombotic status of hypertension patients[62]. However, the related molecular mechanisms were largely unclear. We discovered that GPIbα in hypertension patients are hyperactive and can induce stronger mechanosignaling, while a substantial amount of integrin $\alpha_{IIb}\beta_3$ molecules are already in the E^+ status, which together result in an over-expression of E^+ integrin $\alpha_{IIb}\beta_3$ in the patients' biomechanical thrombi. Considering the central roles of GPIbα and E^+ integrin $\alpha_{IIb}\beta_3$ in biomechanical platelet aggregation[12], these results explain the intensified biomechanical thrombogenesis observed in hypertension patients' blood, and suggest that GPIbα-integrin $\alpha_{IIb}\beta_3$ mechanosensing axis hyperactivity directly contributes to the high incidence rate of CVD in hypertension patients. On the other hand, antiplatelet resistance is conventionally believed to be due to patients' lack of sensitivity to antiplatelets in inhibiting platelet amplification loops[63]. However, we found that biomechanical thrombogenesis is essentially "immune" to aspirin and clopidogrel in both healthy young subjects and hypertension patients (Supp. Fig. 10). These, together with similar observations by other works[10,12,32], indicate a new mechanism of antiplatelet resistance: biomechanical platelet aggregation can mediate arterial thrombosis independent of platelet amplification mechanisms, and therefore the sole inhibition of platelet amplification loops allows thrombotic risks to persist by leaving biomechanical platelet aggregation active. Altogether, our results strongly advocate the development of GPIbα and/or integrin $\alpha_{IIb}\beta_3$ targeting anti-thrombotic 'mechanomedicines' that can work complementarily with conventional antiplatelets for enhanced treatment efficacy. The results also underscore the (patho)physiological relevance of integrin E^+-closed conformation,

which should inspire future investigations on the importance of the E^+-closed conformation in other integrins and in the context of other diseases. The cause of GPIbα and integrin $\alpha_{IIb}\beta_3$ hyperactivity in hypertension patients warrants further investigation, which is possibly relevant to hypertension-associated oxidative stress and inflammation[64,65], dysregulated glycosylation of the receptors by metabolic complications[66], and/or the activation of mechanosensitive ion channel Piezo1[16].

P-selectin and Act. $\alpha_{IIb}\beta_3$ are widely used markers of platelet activation, but their performance in diagnosing thrombosis is unsatisfactory due to low sensitivty[67]. We show that E^+ $\alpha_{IIb}\beta_3$ has a much better performance than P-selectin and Act. $\alpha_{IIb}\beta_3$ in correlating with the biomechanical thrombus size and in separating healthy young subjects and subjects carrying thrombotic risk factors. Furthermore, only E^+ $\alpha_{IIb}\beta_3$, but not P-selectin or Act. $\alpha_{IIb}\beta_3$, was detected on platelets freshly isolated from hypertension patients. These results underscore the accuracy and sensitivity of E^+ $\alpha_{IIb}\beta_3$ in detecting platelet hyperreactivity, suggesting its use as an independent biomarker for predicting arterial thrombosis in certain populations.

Over the past decades, a widespread routine has formed to evaluate the efficacy of new anti-thrombotic strategies solely based on thrombus size reduction and without considering inter-individual variability[11,68]. Our work demonstrates that thrombi possess multi-dimensional characteristics that can be orthogonal, which should be summarized as a 'profile' or a 'barcode'. Because different individuals have differential personal thrombus barcodes, and different anti-thrombotics have differential effect barcodes, a treatment mismatch can easily occur. Conceptually distinguished from antiplatelet resistance, a drug with treatment mismatch is still effective in reducing the thrombus size, but has limited or undesired effects on the thrombus composition and/or activation status (Supp. Fig. 11). The life-threatening danger of treatment mismatch has been documented in multiple phase III trials where conventional integrin $\alpha_{IIb}\beta_3$ antagonists (e.g., orbofiban), despite high potency in inhibiting soluble agonist-induced platelet aggregation (and also biomechanical platelet aggregation as demonstrated in this work), paradoxically increased patient mortality by enhancing the risk of myocardial infarction[69,70]. It was later realized that the failure of these drugs was associated with their effect of stimulating integrin $\alpha_{IIb}\beta_3$ activation, which likely causes relapse of thrombosis[71]. Addressing this issue, a chemical principle was recently discovered to develop anti-thrombotic candidates that lock

integrin $\alpha_{IIb}\beta_3$ in the inactive state[72]. Developing diversified anti-thrombotics and determining their effect barcodes and their interactions with thrombosis-exacerbating factors can help avoid treatment mismatch, in which the 'addition rule' could be greatly helpful for prediction. The inter-individual variability in drug efficacy further urges the personalized selection of anti-thrombotics for treatment optimization.

MATERIALS AND METHODS

Study design

This study was designed to develop a translational multi-parametric platform that characterizes thrombogenesis in the arterial biomechanical settings. Based on previously developed stenosis flow chamber assay, we incorporated multi-fluorescence imaging to concurrently monitor the size, composition and activation status of the thrombus, together reporting a 'thrombus profile'. After validating the feasibility of this thrombus profiling assay, we validated that the assay can distinguish the effects of anti-thrombotic antibodies with different targets. To assess whether the assay could detect higher risks of arterial thrombosis, we applied blood samples from hypertensive and older people and detected multi-dimensional thrombus abnormality that is featured by a significantly higher expression of activated integrin $\alpha_{IIb}\beta_3$. Further analysis was conducted to explore the correlation between thrombus abnormality and the subjects' health conditions (blood pressure level, duration of hypertension, etc.) and demographics other than age. With prior evidence indicating a central role of activated integrin $\alpha_{IIb}\beta_3$ in biomechanical thrombogenesis, we further employed 4 additional experimental approaches and investigated the molecular mechanisms underlying the integrin $\alpha_{IIb}\beta_3$ over-activation in hypertension patients' thrombi. Lastly, we studied how different anti-thrombotic agents affect the thrombus profile of hypertension patients, and whether personal thrombus profiles have high inter-individual variability. Due to the nature of this study, randomization was not done. No statistical methods were used to predetermine sample sizes (n), which are indicated in the figures and legends. The investigators who collected blood samples and performed experiments and those who analyzed the experimental data were always separate. The investigators who analyzed the data were blinded to the detailed information of the subject until the analysis was complete.

Reagents

SZ22-FITC and P2-Alexa Fluor® 488 (Beckman Coulter), AK4-Alexa Fluor® 647 and PAC-1-Alexa Fluor® 647 (BioLegend), AK2, HIP-8-Alexa Fluor 488, Annexin V-Pacific Blue, Annexin V-Alexa Fluor® 488, heparin, $DiOC_6(3)$ and Alexa Fluor® 405, 555 and 647 conjugation kits (ThermoFisher Scientific, MBC 370.2 (Kerafast), fibrinogen (Innovative Research), NMC4, 2.2.9, LJ-P5, 152B6, LJ-155B39, LJ-134B29 and VWFA1[73] (MERU VasImmune), VWF monomer (Sino Biological), and PS-CNP beads (Bangs Laboratories) were purchased. 7E9, 7E3 and 10E5 were gifts from Barry S. Coller (Rockefeller University).

Human subjects

All procedures involving human subjects were approved by the Institutional Review Board of the University of Texas Medical Branch (protocol number: 22-0015) and the University of Sydney (ethics reference number: 2023/582). Informed consent was obtained from all subjects.

Subject number (n) and age (mean±s.d.): healthy young: n =33, age =34.0±6.3; healthy older: n =10, age =63.8±11.3; hypertensive young: n =9, age =36.1±8.7; hypertensive older: n =13, age =60.2±9.4. All groups contained both male and female subjects with multiple races and both non-Hispanic/Latino and Hispanic/Latino ethnicities.

All hypertension patients were taking prescribed hypertension medications (e.g., prazosin, amlodipine, enalapril). Patients taking other medications or under the treatment for other diseases within 2 weeks before the blood draw were excluded from this study.

Blood collection, reconstitution and platelet isolation

For whole blood stenosis assay, blood was slowly drawn from the vein of a volunteer into a syringe pre-loaded with heparin (20 U/mL).

For laminar flow chamber assay, BFP assays and flow cytometry, blood was drawn into a syringe pre-loaded with ACD buffer. Then blood reconstitution[73] was performed for laminar flow chamber assay to deplete plasma and reach a hematocrit of 45% and platelet count of 20,000 μL^{-1}. Or, platelet isolation was performed for BFP assays and flow cytometry[12], with

platelets finally resuspended in modified Tyrode's buffer (135 mM NaCl, 11.9 mM $NaHCO_3$, 2.9 mM KCl, 0.42 mM NaH_2PO_4, 10 mM Hepes, 5.5 mM dextrose, pH 7.4).

Microfluidic device preparation

Polydimethylsiloxane (PDMS) was applied on a silicon mold (1-μm resolution), which was heated at 75°C for 1 h for curing, peeled off and cut into single pieces. Holes were drilled to create outlets and inlets. The devices then underwent plasma treatment and were bonded to glass coverslips.

Microfluidic stenosis assay

Microfluidic channels were coated with VWF monomer (2 μg mL^{-1}) for 1 h. Heparinized whole blood was incubated with $DiOC_6(3)$ (5 μM) for 1 minute, or with Sensor Set 1 (SZ22-FITC (0.5 μg mL^{-1}), Fg-Alexa Fluor® 405 (60 μg mL^{-1}), 2.2.9-Alexa Fluor® 555 (1 μg mL^{-1}) and AK4-Alexa Fluor® 647 (1 μg mL^{-1})) or Set 2 (SZ22-FITC (0.5 μg mL^{-1}), Annexin V-Pacific Blue (1 μg mL^{-1}), MBC 370.2-Alexa Fluor® 555 (1 μg mL^{-1}) and PAC-1-Alexa Fluor® 647 (1 μg mL^{-1})) for 10 min, and perfused through the channel. Thrombus formation was observed using a Leica DM IL LED microscope (camera: Leica DFC360 FX; objective lens: air, 20×; acquisition software: LAS X). No bleed-through between fluorescence channels was observed. Platelet autofluorescence was detected in 391-nm channel[74], which was subtracted when calculating signals.

In some experiments, different concentrations of aspirin (with 15 μg mL^{-1} defined as 2×) and/or clopidogrel (with 6 μg mL^{-1} defined as 2×) or ALB cocktail (1 U mL^{-1} apyrase, 100 mM MRS2179, 10 mM 2-MeSAMP, 10 μM indomethacin, 800 U mL^{-1} hirudin) were added into blood to inhibit platelet amplification loops.

Hill equation was used to derive IC50 of inhibitors:

$$\text{Residue size} = R+(100-R)/(1+(\text{IC50}/C)\text{^HillSlope}) \quad (1)$$

wherein C is the inhibitor concentration, R is the residue size when the effect of the inhibitor saturates, and HillSlope is a constant.

For subjects who were tested for multiple times, average values of these test results were used in statistical analysis.

Microfluidic laminar flow chamber assay

Reconstituted blood added with $DiOC_6(3)$ (10 μM) was perfused at different shear rates over straight channels pre-coated with VWFA1 or fibrinogen. After 5 min, fluorescent signals from platelets were recorded at 40 frame s^{-1}.

Biomembrane force probe (BFP) and fluorescence BFP (fBFP)

In a chamber filled with modified Tyrode's buffer + 0.5% BSA (plus 1 mM Ca^{2+}/Mg^{2+} when interrogating platelets with Fg beads), a streptavidin-coated glass probe bead was glued to the apex of a biotinylated RBC, which is aspirated by a micropipette to form an ultra-sensitive force probe[51]. The probe bead was also coated with VWFA1 or Fg. On the opposing target side, a freshly isolated platelet was aspirated by a second micropipette, which was driven by a piezoelectric translator (Physical Instrument) to repeatedly bring the platelet in and out of contact with the bead to form adhesion events. The bead was monitored under an inverted microscope (IX83, Olympus) by a high-speed camera. A custom image analysis LabView (National Instrument) program tracks the bead position with 3 nm precision in real-time. The BFP spring constant k was determined by the suction pressure inside the probe pipette and the geometric parameters of the force transducer assembly[75].

For adhesion frequency assay, the platelet was repeatedly brought into contact with the probe bead for 2 seconds and retracted. Adhesion events were signified by the elongation of the RBC upon platelet retraction, which yielded a tensile force signal on the bead. Adhesion and non-adhesion events in 30 cycles were enumerated to calculate adhesion frequency, P_a. The effective avidity ($A_cK_am_r$) and affinity (A_cK_a) were derived by the following equation[52],

$$P_a = 1 - \exp\{-m_r m_l A_c K_a\} \quad (2)$$

where m_r and m_l are the receptor and ligand surface densities derived from flow cytometry.

For force-clamp assay, contact time was shortened until achieving infrequent (~20%) adhesion, which ensures that most (~90%) of the adhesion events are mediated by single

receptor-ligand bonds. Once an adhesion event was observed, the platelet would be held at a desired clamping force to wait for the bond to dissociate[51]. Lifetime was determined as the time from the instant when the force reached the desired level to the instant of bond dissociation. The collected lifetimes were categorized into bins that cover successive force ranges. The average lifetime in each force bin was calculated to plot the "lifetime *vs*. clamping force" curve.

For fBFP, platelets were pre-loaded with Fura-2-AM and interrogated by VWFA1 beads with the force-clamp assay mode, but the contact time was kept at 2 seconds. Ratiometric imaging with a light source that alternates between 340 nm (to excite Ca^{2+}-engaged Fura-2) and 380 nm (to excite Ca^{2+}-free Fura-2) was used to measure the Ca^{2+} level in the aspirated platelet[54]. Signal intensity from the 340-nm channel was divided by that from the 380-nm channel and then normalized by the average value of the first 10 frames to derive the normalized Ca^{2+} level.

Flow cytometry assay

Platelet suspension was incubated with 2 μg mL^{-1} of HIP-8-Alexa Fluor® 488, MBC370.2-Alexa Fluor® 555, PAC-1-Alexa Fluor® 647 or AK4-Alexa Fluor® 647 for 10 min, diluted with Hepes-Tyrode buffer by 10 times, and immediately analyzed by flow cytometry.

Statistical Analysis

Statistical significance of the differences between two groups was determined by Student *t*-test. For multi-group analysis, 1-way or 2-way ANOVA was used. When significant differences were shown, data was subjected to Turkey test for multiple comparisons. Regression slope test was used to assess whether the slope of a linear fitting is significantly non-zero. Spearman rank correlation coefficient[47] and Kendall's tau correlation coefficient[48] were also used to test whether a positive correlation exists between different readouts of the thrombus profile. P-values <0.05 were considered significant.

List of Supplementary Information

Supplementary Methods

Figures S1 to S11

Tables S1 to S3

Data Availability

All data supporting the findings of this study are available within the article and its supplementary files. Any additional requests for information can be directed to, and will be fulfilled by, the corresponding authors. Source data are provided with this paper.

References

1 Benjamin, E. J. *et al.* Heart Disease and Stroke Statistics-2019 Update: A Report From the American Heart Association. *Circulation* **139**, e56-e528, doi:10.1161/CIR.0000000000000659 (2019).

2 Springer, T. A. von Willebrand factor, Jedi knight of the bloodstream. *Blood* **124**, 1412-1425, doi:10.1182/blood-2014-05-378638 (2014).

3 Akturk, I. F. *et al.* Hypertension as a risk factor for aspirin and clopidogrel resistance in patients with stable coronary artery disease. *Clin Appl Thromb Hemost* **20**, 749-754, doi:10.1177/1076029613481102 (2014).

4 Liu, X. F. *et al.* Prevalence of and risk factors for aspirin resistance in elderly patients with coronary artery disease. *J Geriatr Cardiol* **10**, 21-27, doi:10.3969/j.issn.1671-5411.2013.01.005 (2013).

5 Jackson, S. P. Arterial thrombosis--insidious, unpredictable and deadly. *Nature medicine* **17**, 1423-1436, doi:10.1038/nm.2515 (2011).

6 Previtali, E., Bucciarelli, P., Passamonti, S. M. & Martinelli, I. Risk factors for venous and arterial thrombosis. *Blood Transfus* **9**, 120-138, doi:10.2450/2010.0066-10 (2011).

7 Govender, R. D., Al-Shamsi, S., Soteriades, E. S. & Regmi, D. Incidence and risk factors for recurrent cardiovascular disease in middle-eastern adults: a retrospective study. *BMC Cardiovasc Disord* **19**, 253, doi:10.1186/s12872-019-1231-z (2019).

8 Zhang, Y. *et al.* Emerging Microfluidic Approaches for Platelet Mechanobiology and Interplay With Circulatory Systems. *Front Cardiovasc Med* **8**, 766513, doi:10.3389/fcvm.2021.766513 (2021).

9 Zhang, Y., Jiang, F., Chen, Y. & Ju, L. A. Platelet Mechanobiology Inspired Microdevices: From Hematological Function Tests to Disease and Drug Screening. *Frontiers in pharmacology* **12**, 779753, doi:10.3389/fphar.2021.779753 (2021).

10 Nesbitt, W. S. *et al.* A shear gradient-dependent platelet aggregation mechanism drives thrombus formation. *Nature medicine* **15**, 665-673, doi:10.1038/nm.1955 (2009).

11 Chen, Y. & Ju, L. A. Biomechanical thrombosis: the dark side of force and dawn of mechano-medicine. *Stroke Vasc Neurol* **5**, 185-197, doi:10.1136/svn-2019-000302 (2020).

12 Chen, Y. *et al.* An integrin alphaIIbbeta3 intermediate affinity state mediates biomechanical platelet aggregation. *Nature materials* **18**, 760-769, doi:10.1038/s41563-019-0323-6 (2019).

13 Fu, H. *et al.* Flow-induced elongation of von Willebrand factor precedes tension-dependent activation. *Nature communications* **8**, 324, doi:10.1038/s41467-017-00230-2 (2017).

14 Yago, T. *et al.* Platelet glycoprotein Ibalpha forms catch bonds with human WT vWF but not with type 2B von Willebrand disease vWF. *The Journal of clinical investigation* **118**, 3195-3207, doi:10.1172/JCI35754 (2008).

15 Ju, L. *et al.* Compression force sensing regulates integrin alphaIIbbeta3 adhesive function on diabetic platelets. *Nature communications* **9**, 1087, doi:10.1038/s41467-018-03430-6 (2018).
16 Zhao, W. *et al.* Piezo1 initiates platelet hyperreactivity and accelerates thrombosis in hypertension. *Journal of thrombosis and haemostasis : JTH*, doi:10.1111/jth.15504 (2021).
17 Ju, L. A. *et al.* Microfluidic post method for 3-dimensional modeling of platelet-leukocyte interactions. *Analyst* **147**, 1222-1235, doi:10.1039/d2an00270a (2022).
18 Zhang, X. F. & Cheng, X. Platelet mechanosensing axis revealed. *Nature materials* **18**, 661-662, doi:10.1038/s41563-019-0393-5 (2019).
19 Yakusheva, A. A. *et al.* Traumatic vessel injuries initiating hemostasis generate high shear conditions. *Blood advances* **6**, 4834-4846, doi:10.1182/bloodadvances.2022007550 (2022).
20 Panteleev, M. A. *et al.* Wall shear rates in human and mouse arteries: Standardization of hemodynamics for in vitro blood flow assays: Communication from the ISTH SSC subcommittee on biorheology. *Journal of thrombosis and haemostasis : JTH* **19**, 588-595, doi:10.1111/jth.15174 (2021).
21 Dent, J. A., Galbusera, M. & Ruggeri, Z. M. Heterogeneity of plasma von Willebrand factor multimers resulting from proteolysis of the constituent subunit. *The Journal of clinical investigation* **88**, 774-782, doi:10.1172/JCI115376 (1991).
22 Kamath, S., Blann, A. D. & Lip, G. Y. Platelet activation: assessment and quantification. *European heart journal* **22**, 1561-1571, doi:10.1053/euhj.2000.2515 (2001).
23 Schoenwaelder, S. M. *et al.* Two distinct pathways regulate platelet phosphatidylserine exposure and procoagulant function. *Blood* **114**, 663-666, doi:10.1182/blood-2009-01-200345 (2009).
24 Brazilek, R. J. *et al.* Application of a strain rate gradient microfluidic device to von Willebrand's disease screening. *Lab on a chip* **17**, 2595-2608, doi:10.1039/c7lc00498b (2017).
25 Merten, M., Chow, T., Hellums, J. D. & Thiagarajan, P. A new role for P-selectin in shear-induced platelet aggregation. *Circulation* **102**, 2045-2050, doi:10.1161/01.cir.102.17.2045 (2000).
26 Deng, W. *et al.* Platelet clearance via shear-induced unfolding of a membrane mechanoreceptor. *Nature communications* **7**, 12863, doi:10.1038/ncomms12863 (2016).
27 Hu, H. *et al.* Platelet-leukocyte aggregation under shear stress: differential involvement of selectins and integrins. *Thromb Haemost* **90**, 679-687, doi:10.1160/TH03-05-0274 (2003).
28 Roka-Moiia, Y. *et al.* Platelet Activation via Shear Stress Exposure Induces a Differing Pattern of Biomarkers of Activation versus Biochemical Agonists. *Thromb Haemost* **120**, 776-792, doi:10.1055/s-0040-1709524 (2020).
29 Pang, A. *et al.* Shear-induced integrin signaling in platelet phosphatidylserine exposure, microvesicle release, and coagulation. *Blood* **132**, 533-543, doi:10.1182/blood-2017-05-785253 (2018).
30 Chen, W. *et al.* Inhibiting GPIbalpha Shedding Preserves Post-Transfusion Recovery and Hemostatic Function of Platelets After Prolonged Storage. *Arteriosclerosis, thrombosis, and vascular biology* **36**, 1821-1828, doi:10.1161/ATVBAHA.116.307639 (2016).
31 Arrebola, M. M. *et al.* In vitro effects of clopidogrel on the platelet-subendothelium interaction, platelet thromboxane and endothelial prostacyclin production, and nitric oxide synthesis. *J Cardiovasc Pharmacol* **43**, 74-82, doi:10.1097/00005344-200401000-00012 (2004).

32 Li, M., Hotaling, N. A., Ku, D. N. & Forest, C. R. Microfluidic thrombosis under multiple shear rates and antiplatelet therapy doses. *PloS one* **9**, e82493, doi:10.1371/journal.pone.0082493 (2014).
33 Kanaji, S. *et al.* Humanized GPIbalpha-von Willebrand factor interaction in the mouse. *Blood advances* **2**, 2522-2532, doi:10.1182/bloodadvances.2018023507 (2018).
34 Yuan, Y. *et al.* The von Willebrand factor-glycoprotein Ib/V/IX interaction induces actin polymerization and cytoskeletal reorganization in rolling platelets and glycoprotein Ib/V/IX-transfected cells. *The Journal of biological chemistry* **274**, 36241-36251, doi:10.1074/jbc.274.51.36241 (1999).
35 De Marco, L., Girolami, A., Zimmerman, T. S. & Ruggeri, Z. M. von Willebrand factor interaction with the glycoprotein IIb/IIa complex. Its role in platelet function as demonstrated in patients with congenital afibrinogenemia. *The Journal of clinical investigation* **77**, 1272-1277, doi:10.1172/JCI112430 (1986).
36 Berliner, S., Niiya, K., Roberts, J. R., Houghten, R. A. & Ruggeri, Z. M. Generation and characterization of peptide-specific antibodies that inhibit von Willebrand factor binding to glycoprotein IIb-IIIa without interacting with other adhesive molecules. Selectivity is conferred by Pro1743 and other amino acid residues adjacent to the sequence Arg1744-Gly1745-Asp1746. *The Journal of biological chemistry* **263**, 7500-7505 (1988).
37 Lengweiler, S. *et al.* Preparation of monoclonal antibodies to murine platelet glycoprotein IIb/IIIa (alphaIIbbeta3) and other proteins from hamster-mouse interspecies hybridomas. *Biochemical and biophysical research communications* **262**, 167-173, doi:10.1006/bbrc.1999.1172 (1999).
38 Felding-Habermann, B., Ruggeri, Z. M. & Cheresh, D. A. Distinct biological consequences of integrin alpha v beta 3-mediated melanoma cell adhesion to fibrinogen and its plasmic fragments. *The Journal of biological chemistry* **267**, 5070-5077 (1992).
39 Rooney, M. M., Farrell, D. H., van Hemel, B. M., de Groot, P. G. & Lord, S. T. The contribution of the three hypothesized integrin-binding sites in fibrinogen to platelet-mediated clot retraction. *Blood* **92**, 2374-2381 (1998).
40 Liu, Q., Matsueda, G., Brown, E. & Frojmovic, M. The AGDV residues on the gamma chain carboxyl terminus of platelet-bound fibrinogen are needed for platelet aggregation. *Biochimica et biophysica acta* **1343**, 316-326, doi:10.1016/s0167-4838(97)00130-1 (1997).
41 Sanchez-Cortes, J. & Mrksich, M. The platelet integrin alphaIIbbeta3 binds to the RGD and AGD motifs in fibrinogen. *Chem Biol* **16**, 990-1000, doi:10.1016/j.chembiol.2009.08.012 (2009).
42 Coller, B. S. A new murine monoclonal antibody reports an activation-dependent change in the conformation and/or microenvironment of the platelet glycoprotein IIb/IIIa complex. *The Journal of clinical investigation* **76**, 101-108, doi:10.1172/JCI111931 (1985).
43 Kaul, D. K. *et al.* Monoclonal antibodies to alphaVbeta3 (7E3 and LM609) inhibit sickle red blood cell-endothelium interactions induced by platelet-activating factor. *Blood* **95**, 368-374 (2000).
44 Griffin, M. T., Zhu, Y., Liu, Z., Aidun, C. K. & Ku, D. N. Inhibition of high shear arterial thrombosis by charged nanoparticles. *Biomicrofluidics* **12**, 042210, doi:10.1063/1.5025349 (2018).
45 Wilkerson, W. R. & Sane, D. C. Aging and thrombosis. *Seminars in thrombosis and hemostasis* **28**, 555-568, doi:10.1055/s-2002-36700 (2002).
46 Tsao, C. W. *et al.* Heart Disease and Stroke Statistics-2022 Update: A Report From the

American Heart Association. *Circulation* **145**, e153-e639, doi:10.1161/CIR.0000000000001052 (2022).
47 Charles, S. The proof and measurement of association between two things. *The American Journal of Psychology* **15**, 72–101 (1904).
48 Kendall, M. G. A New Measure of Rank Correlation. *Biometrika* **30**, 81-93 (1938).
49 Safford, M. M. *et al.* Association of race and sex with risk of incident acute coronary heart disease events. *Jama* **308**, 1768-1774, doi:10.1001/jama.2012.14306 (2012).
50 Colantonio, L. D. *et al.* Black-White Differences in Incident Fatal, Nonfatal, and Total Coronary Heart Disease. *Circulation* **136**, 152-166, doi:10.1161/CIRCULATIONAHA.116.025848 (2017).
51 Chen, Y. *et al.* Fluorescence Biomembrane Force Probe: Concurrent Quantitation of Receptor-ligand Kinetics and Binding-induced Intracellular Signaling on a Single Cell. *Journal of visualized experiments*, e52975, doi:10.3791/52975 (2015).
52 Chesla, S. E., Selvaraj, P. & Zhu, C. Measuring two-dimensional receptor-ligand binding kinetics by micropipette. *Biophysical journal* **75**, 1553-1572, doi:10.1016/S0006-3495(98)74074-3 (1998).
53 Ju, L. *et al.* Von Willebrand factor-A1 domain binds platelet glycoprotein Ibalpha in multiple states with distinctive force-dependent dissociation kinetics. *Thrombosis research* **136**, 606-612, doi:10.1016/j.thromres.2015.06.019 (2015).
54 Ju, L., Chen, Y., Xue, L., Du, X. & Zhu, C. Cooperative unfolding of distinctive mechanoreceptor domains transduces force into signals. *eLife* **5**, e15447, doi:10.7554/eLife.15447 (2016).
55 Du, J., Kim, D., Alhawael, G., Ku, D. N. & Fogelson, A. L. Clot Permeability, Agonist Transport, and Platelet Binding Kinetics in Arterial Thrombosis. *Biophysical journal* **119**, 2102-2115, doi:10.1016/j.bpj.2020.08.041 (2020).
56 Wong, N. D. *et al.* Atherosclerotic cardiovascular disease risk assessment: An American Society for Preventive Cardiology clinical practice statement. *Am J Prev Cardiol* **10**, 100335, doi:10.1016/j.ajpc.2022.100335 (2022).
57 Anjum, M. *et al.* Stroke and bleeding risk in atrial fibrillation with CHA2DS2-VASC risk score of one: the Norwegian AFNOR study. *European heart journal* **45**, 57-66, doi:10.1093/eurheartj/ehad659 (2024).
58 Mahalingam, A. *et al.* Numerical analysis of the effect of turbulence transition on the hemodynamic parameters in human coronary arteries. *Cardiovasc Diagn Ther* **6**, 208-220, doi:10.21037/cdt.2016.03.08 (2016).
59 Jackson, S. P. The growing complexity of platelet aggregation. *Blood* **109**, 5087-5095, doi:10.1182/blood-2006-12-027698 (2007).
60 Dai, K., Bodnar, R., Berndt, M. C. & Du, X. A critical role for 14-3-3zeta protein in regulating the VWF binding function of platelet glycoprotein Ib-IX and its therapeutic implications. *Blood* **106**, 1975-1981, doi:10.1182/blood-2005-01-0440 (2005).
61 Shen, B. *et al.* A directional switch of integrin signalling and a new anti-thrombotic strategy. *Nature* **503**, 131-135, doi:10.1038/nature12613 (2013).
62 Gkaliagkousi, E., Passacquale, G., Douma, S., Zamboulis, C. & Ferro, A. Platelet activation in essential hypertension: implications for antiplatelet treatment. *Am J Hypertens* **23**, 229-236, doi:10.1038/ajh.2009.247 (2010).
63 Cattaneo, M. Resistance to anti-platelet agents. *Thrombosis research* **127 Suppl 3**, S61-63, doi:10.1016/S0049-3848(11)70017-2 (2011).

64 Griendling, K. K. *et al.* Oxidative Stress and Hypertension. *Circulation research* **128**, 993-1020, doi:10.1161/CIRCRESAHA.121.318063 (2021).
65 Scherlinger, M., Richez, C., Tsokos, G. C., Boilard, E. & Blanco, P. The role of platelets in immune-mediated inflammatory diseases. *Nature reviews. Immunology* **23**, 495-510, doi:10.1038/s41577-023-00834-4 (2023).
66 Schjoldager, K. T., Narimatsu, Y., Joshi, H. J. & Clausen, H. Global view of human protein glycosylation pathways and functions. *Nature reviews. Molecular cell biology* **21**, 729-749, doi:10.1038/s41580-020-00294-x (2020).
67 Chung, T. *et al.* Platelet activation in acute pulmonary embolism. *Journal of thrombosis and haemostasis : JTH* **5**, 918-924, doi:10.1111/j.1538-7836.2007.02461.x (2007).
68 Gawaz, M., Geisler, T. & Borst, O. Current concepts and novel targets for antiplatelet therapy. *Nature reviews. Cardiology* **20**, 583-599, doi:10.1038/s41569-023-00854-6 (2023).
69 Topol, E. J. *et al.* Randomized, double-blind, placebo-controlled, international trial of the oral IIb/IIIa antagonist lotrafiban in coronary and cerebrovascular disease. *Circulation* **108**, 399-406, doi:10.1161/01.CIR.0000084501.48570.F6 (2003).
70 Chew, D. P., Bhatt, D. L., Sapp, S. & Topol, E. J. Increased mortality with oral platelet glycoprotein IIb/IIIa antagonists: a meta-analysis of phase III multicenter randomized trials. *Circulation* **103**, 201-206, doi:10.1161/01.cir.103.2.201 (2001).
71 Cox, D. *et al.* Evidence of platelet activation during treatment with a GPIIb/IIIa antagonist in patients presenting with acute coronary syndromes. *Journal of the American College of Cardiology* **36**, 1514-1519, doi:10.1016/s0735-1097(00)00919-0 (2000).
72 Lin, F. Y. *et al.* A general chemical principle for creating closure-stabilizing integrin inhibitors. *Cell* **185**, 3533-3550 e3527, doi:10.1016/j.cell.2022.08.008 (2022).
73 Reininger, A. J. *et al.* Mechanism of platelet adhesion to von Willebrand factor and microparticle formation under high shear stress. *Blood* **107**, 3537-3545, doi:10.1182/blood-2005-02-0618 (2006).
74 Lohmann, W. & Lohmann, C. Native fluorescence of platelets from patients with occlusive arterial disease. *Biochemical and biophysical research communications* **152**, 1410-1415, doi:10.1016/s0006-291x(88)80442-x (1988).
75 Evans, E., Ritchie, K. & Merkel, R. Sensitive force technique to probe molecular adhesion and structural linkages at biological interfaces. *Biophysical journal* **68**, 2580-2587, doi:10.1016/S0006-3495(95)80441-8 (1995).

Acknowledgments

We thank B. S. Coller (Rockefeller University) for sharing precious reagents, Y. Wang (The University of Texas Medical Branch) for technical support, and Z. M. Ruggeri (The Scripps Research Institute) for providing valuable suggestions.

Funding:

National Heart, Lung, and Blood Institute grant R00HL153678 (Y.C.)
National Institute on Aging the Claude D. Pepper Older Americans Independence Center Award #P30-AG024832 (Y.C.)
UT System Rising STARs award (Y.C.)
American Heart Association Postdoctoral Fellowship 20POST35080023 (Y.C.)
National Institute of General Medical Sciences grant 1R01GM152812 (L.X.)
National Science Foundation grants DMS-1953189, CCF-2007823 and DMS-2210775 (L.X.)
MRFF Cardiovascular Health Mission Grants APP2016165 and APP2023977 (L.A.J.)
National Heart Foundation Future Leader Fellowship Level 2 (105863) (L.A.J.)
Snow Medical Research Foundation Fellowship 2022SF176 (L.A.J.)

Author contributions:

Methodology: MD, SP, RX, FZ, ZC, YC
Experiments: MD, SP, SU, BC, NAZA, SR, AB, YC
Data analysis: MD, SP, SU, BC, NAZA, SR, AB, HY, LX, RX, FZ
Donor recruitment and blood collection: MD, SP, SU, AB and MB
Funding acquisition: LX, LAJ, YC
Supervision: LAJ, YC
Writing: MD, HY, RX, FZ, NAZA, MM, LH, ZF, CZ, MB, LX, LAJ, YC

Competing interests: Authors declare that they have no competing interests.

Data and materials availability: All data are available in the main text or supplemental materials. For sharing of renewable materials, datasets, and protocols, please contact yunfchen@utmb.edu

Figures

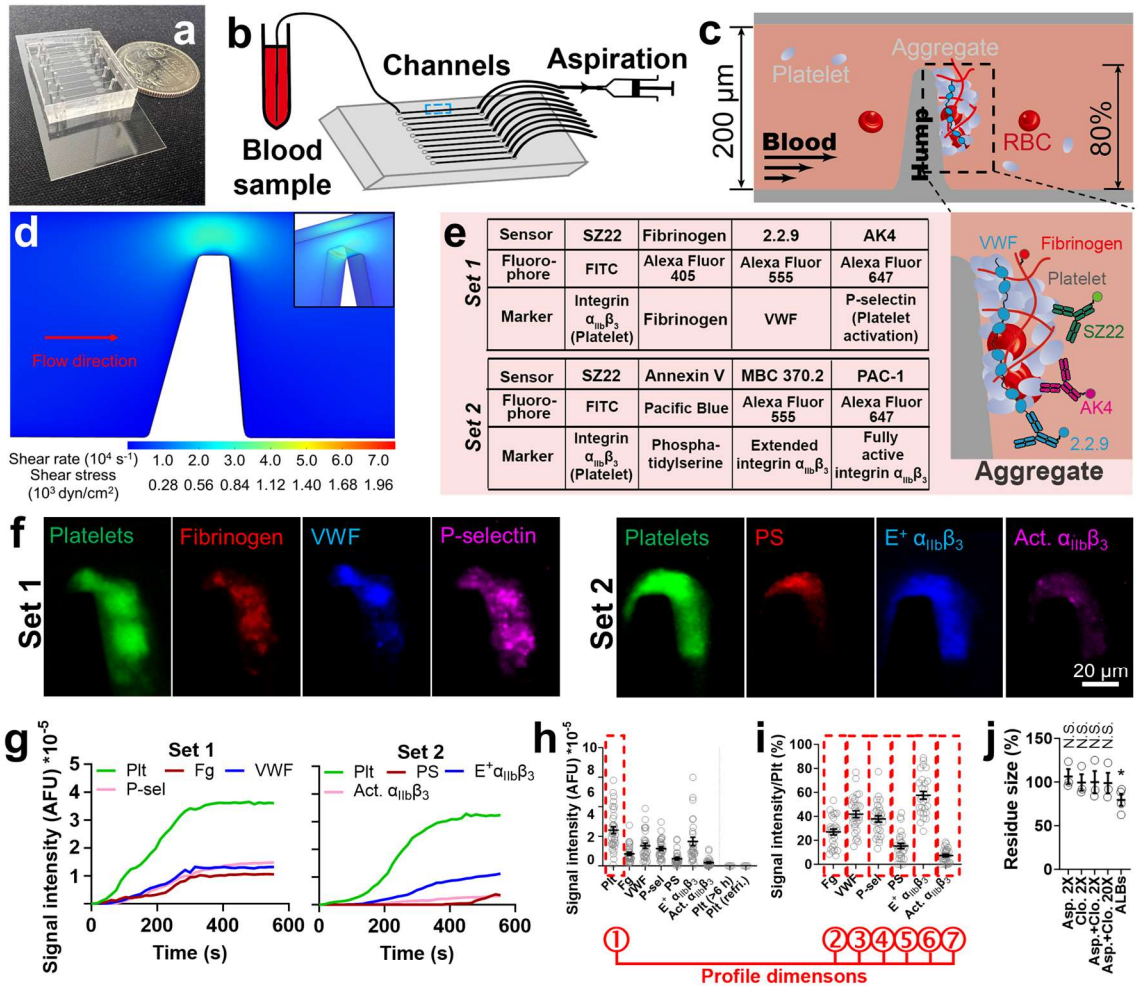

Figure 1. Combining microfluidic stenosis assay with multi-fluorescence imaging to comprehensively characterize biomechanical platelet aggregation. (**a**) A microfluidic chip with a quarter coin placed adjacently. (**b**) Illustration of experimental setup. (**c**) Zoom-in of the dashed box in (b). A hump inside the channel creates 80% stenosis. When blood is perfused over, platelets spontaneously aggregate around the hump. (**d**) Shear rate and shear stress at the stenosis area estimated by fluid dynamics simulation. (**e**) *Left*: a layout of the two sets of fluorescently tagged sensors for thrombus profiling. *Right*: zoom-in of the thrombus shown in (c), illustrating the staining of Sensor Set 1. (**f**) Representative fluorescent images of thrombi stained with Sensor Set 1 (*left*) and 2 (*right*). (**g**) Representative time courses of signal intensity of biomarkers in Sensor Set 1 (*left*, detecting platelets (Plt), fibrinogen (Fg), VWF and P-selectin) and 2 (*right*, detecting platelets, phosphatidylserine (PS), extended integrin $\alpha_{IIb}\beta_3$ (E^+ $\alpha_{IIb}\beta_3$) and fully activated $\alpha_{IIb}\beta_3$ (Act. $\alpha_{IIb}\beta_3$)). AFU: arbitrary fluorescence unit. (**h,i**) Scatter plots with mean±s.e.m. (n =28) of the signal intensity of all biomarkers (h) and the normalized signal intensity of Fg, VWF, P-selectin, PS, E^+ $\alpha_{IIb}\beta_3$ and Act. $\alpha_{IIb}\beta_3$ (i) 7.5 min after the onset of thrombus formation. The definition of each dimension of the 7-dimension thrombus profile is indicated below. (**j**) Scatter plots with mean±s.e.m. (n ≥3) of the thrombus residue size in the presence of aspirin (2×) or clopidogrel (2×) or both (2× or 20×), or ALB cocktail. *p <0.05; N.S., not significant, compared with no drug treatment, assessed by multiple t-test.

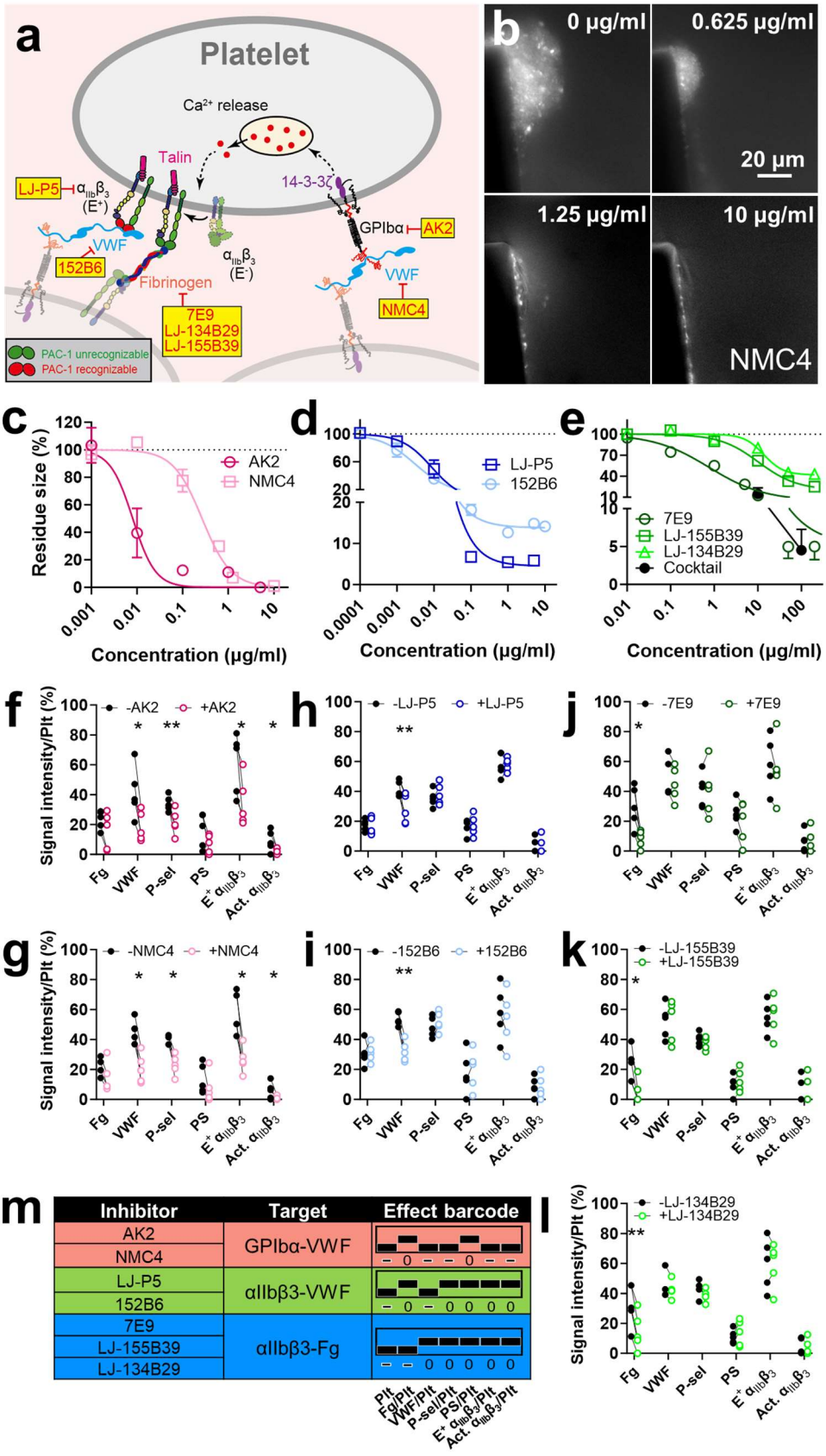
a
Platelet
Ca2+ release
Talin
14-3-3ζ
LJ-P5
αIIbβ3 (E+)
VWF
152B6
αIIbβ3 (E-)
GPIbα
AK2
VWF
NMC4
Fibrinogen
7E9
LJ-134B29
LJ-155B39
PAC-1 unrecognizable
PAC-1 recognizable
b
0 μg/ml
0.625 μg/ml
20 μm
1.25 μg/ml
10 μg/ml
NMC4
c
Residue size (%)
AK2
NMC4
Concentration (μg/ml)
d
LJ-P5
152B6
Concentration (μg/ml)
e
7E9
LJ-155B39
LJ-134B29
Cocktail
Concentration (μg/ml)
f
Signal intensity/Plt (%)
-AK2
+AK2
Fg
VWF
P-sel
PS
E+ αIIbβ3
Act. αIIbβ3
h
-LJ-P5
+LJ-P5
j
-7E9
+7E9
g
-NMC4
+NMC4
i
-152B6
+152B6
k
-LJ-155B39
+LJ-155B39
m
Inhibitor
Target
Effect barcode
AK2
NMC4
GPIbα-VWF
LJ-P5
152B6
αIIbβ3-VWF
7E9
LJ-155B39
LJ-134B29
αIIbβ3-Fg
Plt
Fg/Plt
VWF/Plt
P-sel/Plt
PS/Plt
E+ αIIbβ3/Plt
Act. αIIbβ3/Plt
l
-LJ-134B29
+LJ-134B29

Figure 2. Delineating the respective contribution of GPIbα–VWF, $\alpha_{IIb}\beta_3$–VWF and $\alpha_{IIb}\beta_3$–fibrinogen interactions to biomechanical platelet aggregation. (**a**) Illustration of key receptor–ligand interactions in a biomechanical thrombus, highlighting the GPIbα-integrin $\alpha_{IIb}\beta_3$ mechanosensing axis. A panel of monoclonal antibodies and their respective targets are indicated, which were used to inhibit one receptor or ligand at a time. The head of integrin $\alpha_{IIb}\beta_3$ colored green or red respectively denotes the integrin being unrecognizable or recognizable by PAC-1. (**b**) Representative images of $DiOC_6(3)$-labeled thrombi formed in the presence of different concentrations of NMC4. (**c-e**) Dose-dependency curves of antibodies against GPIbα–VWF (c), $\alpha_{IIb}\beta_3$–VWF (d) and $\alpha_{IIb}\beta_3$–fibrinogen (e) interactions in reducing the size of biomechanical thrombi (mean±s.e.m.). (**f-l**) Comparing the normalized signal intensities of Fg, VWF, P-selectin, PS, E^+ $\alpha_{IIb}\beta_3$ and Act. $\alpha_{IIb}\beta_3$ in the biomechanical thrombi, in the absence and presence of AK2 (f), NMC4 (g), LJ-P5 (h), 152B6 (i), 7E9 (j), LJ-155B39 (k) and LJ-134B29 (l), respectively (mean±s.e.m.; n =5). $*p < 0.05$; $**p < 0.01$, assessed by multiple t-test. (**m**) Summarizing the effects of AK2, NMC4, LJ-P5, 152B6, 7E9, LJ-155B39 and LJ-134B29 on the thrombus profile into 7-digit barcodes. A positive, neutral or negative effect is denoted by a bar being at the top, middle and bottom of the column, respectively; it is also numerically denoted by '+', '0' or '-', respectively. The antibodies are categorized by their target receptor–ligand interaction, which is indicated by different background colors.

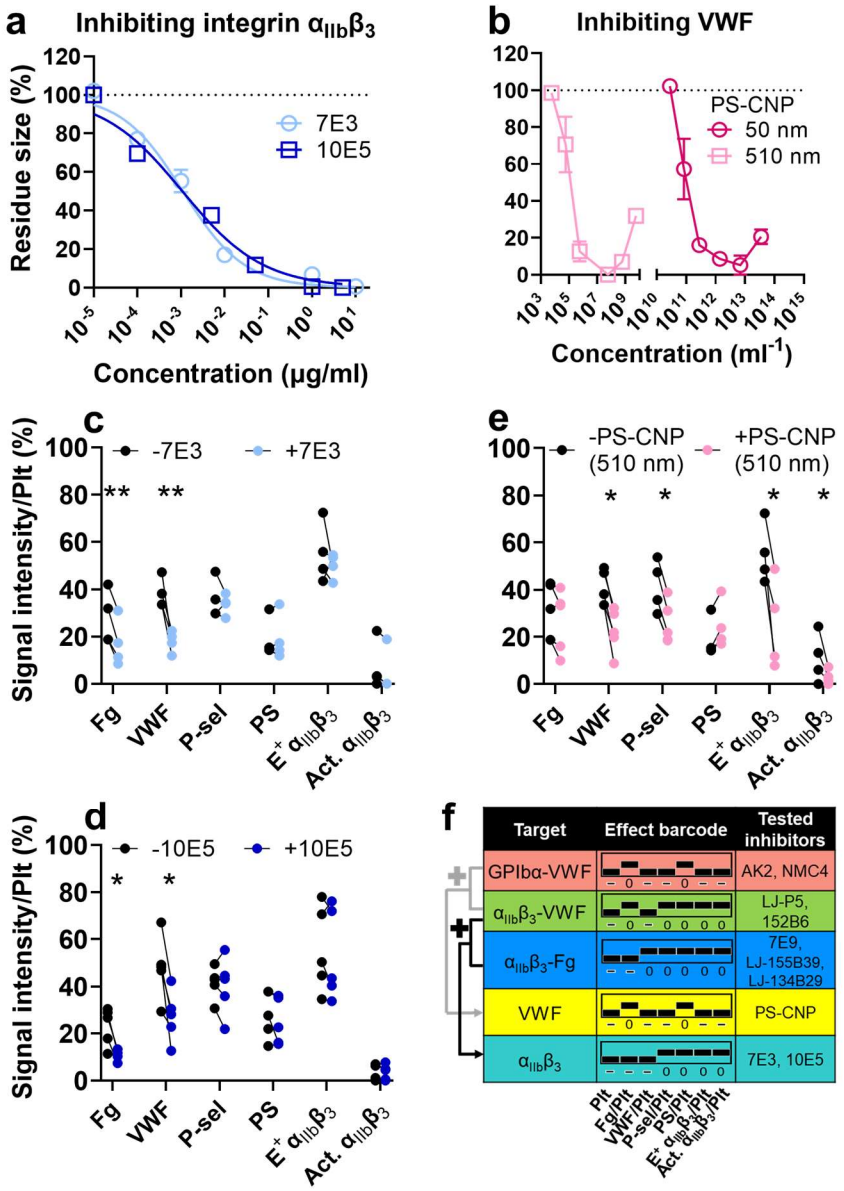

Figure 3. Testing the effects of inhibitors against integrin $\alpha_{IIb}\beta_3$, VWF and soluble agonists on biomechanical platelet aggregation. (**a**) Dose dependency of 7E3 and 10E5, in reducing the size of the biomechanical thrombi (mean±s.e.m.). (**b**) Dose dependency of two sizes (50 and 510 nm) of polystyrene negatively charged nanoparticles (PS-CNP), in reducing the size of the biomechanical thrombi (mean±s.e.m.). (**c-e**) Comparing the normalized signal intensities of Fg, VWF, P-selectin, PS, E^+ $\alpha_{IIb}\beta_3$ and Act. $\alpha_{IIb}\beta_3$ in the biomechanical thrombi, in the absence and presence of 7E3 (c), 10E5 (d) and PS-CNP (diameter: 510 nm) (e), respectively (mean±s.e.m.) (n =4 or 5). *p <0.05; **p <0.01, assessed by multiple t-test. (**f**) Summarizing the 7-digit effect barcodes of 7E3, 10E5 and PS-CNP. A rule of addition is indicated, demonstrating that the add-up of the barcodes of GPIbα–VWF inhibition and $\alpha_{IIb}\beta_3$–VWF inhibition equals that of VWF inhibition, and the add-up of the barcodes of $\alpha_{IIb}\beta_3$–VWF inhibition and $\alpha_{IIb}\beta_3$–Fg inhibition equals that of integrin $\alpha_{IIb}\beta_3$ inhibition.

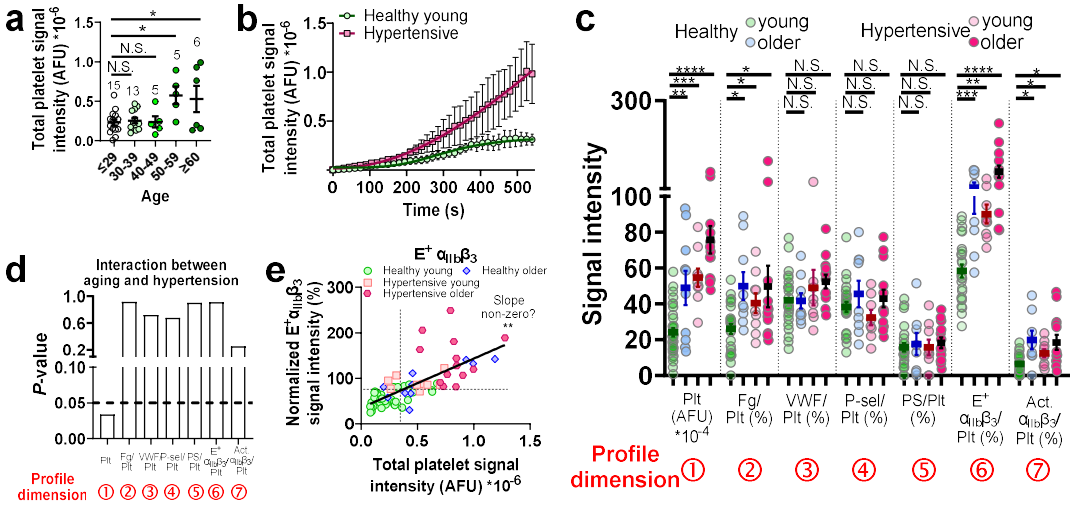
a
Total platelet signal intensity (AFU) *10^-6
Age
b
Healthy young
Hypertensive
Total platelet signal intensity (AFU) *10^-6
Time (s)
c
Healthy young older
Hypertensive young older
Signal intensity
Plt (AFU) *10^-4
Fg/ Plt (%)
VWF/ Plt (%)
P-sel/ Plt (%)
PS/Plt (%)
E+ αIIbβ3/ Plt (%)
Act. αIIbβ3/ Plt (%)
Profile dimension ① ② ③ ④ ⑤ ⑥ ⑦
d
Interaction between aging and hypertension
P-value
Profile dimension ① ② ③ ④ ⑤ ⑥ ⑦
e
E+ αIIbβ3
Healthy young
Healthy older
Hypertensive young
Hypertensive older
Slope non-zero?
Normalized E+αIIbβ3 signal intensity (%)
Total platelet signal intensity (AFU) *10^-6

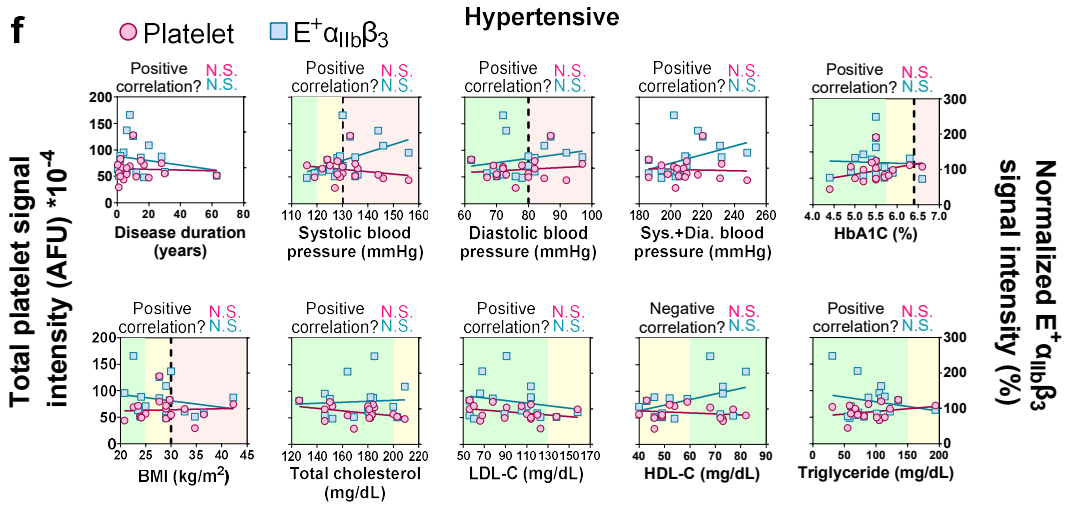
f
Platelet
E+αIIbβ3
Hypertensive
Total platelet signal intensity (AFU) *10^-4
Normalized E+αIIbβ3 signal intensity (%)
Positive correlation? N.S. N.S.
Negative correlation? N.S. N.S.
Disease duration (years)
Systolic blood pressure (mmHg)
Diastolic blood pressure (mmHg)
Sys.+Dia. blood pressure (mmHg)
HbA1C (%)
BMI (kg/m2)
Total cholesterol (mg/dL)
LDL-C (mg/dL)
HDL-C (mg/dL)
Triglyceride (mg/dL)

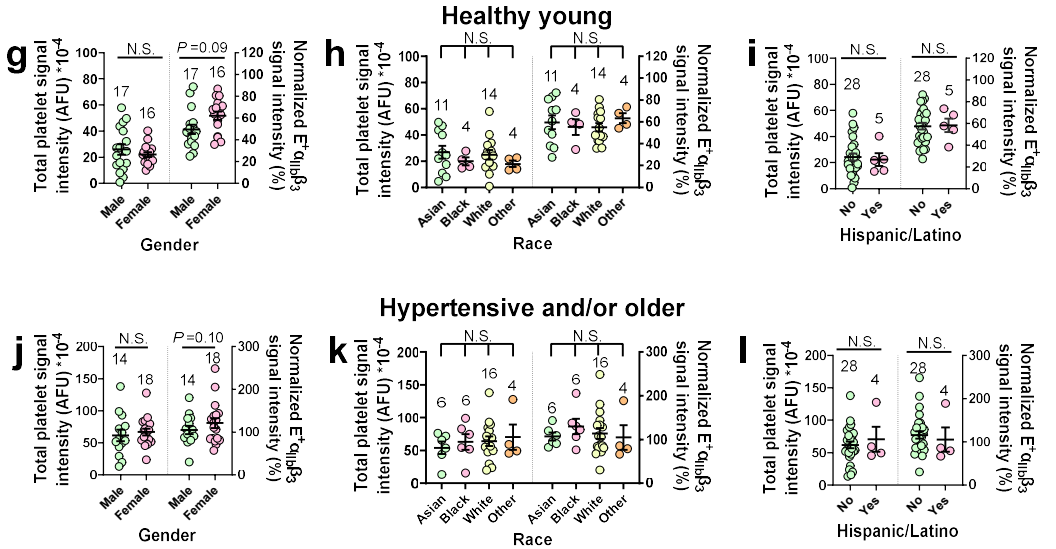
Healthy young
g
h
i
Total platelet signal intensity (AFU) *10^-4
Normalized E+αIIbβ3 signal intensity (%)
N.S.
P=0.09
Male
Female
Gender
Asian
Black
White
Other
Race
No
Yes
Hispanic/Latino
Hypertensive and/or older
j
k
l
P=0.10

Figure 4. Characterizing abnormalities in the thrombus profiles associated with hypertension and aging. (**a**) Scatter plots with mean±s.e.m. (n indicated above each column) of the size of thrombi generated by healthy subjects grouped by age. (**b**) Comparing the time course of thrombus growth (mean±s.e.m. with fitting lines of sigmoidal model) between healthy young and hypertensive groups (n =8). (**c**) Scatter plots with mean±s.e.m. of the thrombus profiles of healthy young, healthy older hypertensive young, and hypertensive older adult subjects (n =33, 10, 9 and 13, respectively). N.S., not significant; **p* <0.05; ***p* <0.01; ****p* <0.001; *****p* <0.0001, assessed by two-way ANOVA. (**d**) *P*-values of the significance of the interaction between aging and hypertension in their impact on the thrombus profile. (**e**) Scatter plot of normalized E^+ $\alpha_{IIb}\beta_3$ signal intensity vs. thrombus size, with blood from healthy young, healthy older, hypertensive young, and hypertensive older subjects (n =33, 10, 9, 13, respectively). Solid line: linear fitting of all data points, with regression slope test used to assess whether the slope is significantly non-zero. Dash lines: threshold values that best separate healthy young and other groups. (**f**) Scatter plots and linear fits of thrombus size and normalized E^+ $\alpha_{IIb}\beta_3$ signal intensity vs. hypertension duration, systolic and diastolic blood pressures and their sum, HbA1C, BMI, total cholesterol, LDL-C, HDL-C and triglyceride in hypertension patients. Green, yellow, and red background colors indicate normal, borderline abnormal and pathologically abnormal ranges, respectively. (**g-l**) Scatter plots with mean±s.e.m. (n indicated above each column) of the thrombus size (*left*) and normalized E^+ $\alpha_{IIb}\beta_3$ signal intensity (*right*) of healthy young (g-i) or hypertensive and/or older (j-l) subjects, grouped by gender (g,j), race (h,k) and ethnicity (i,l). a,g-l: N.S., not significant; ***p* <0.01; *****p* <0.0001, assessed by one-way ANOVA or Student's t-test.

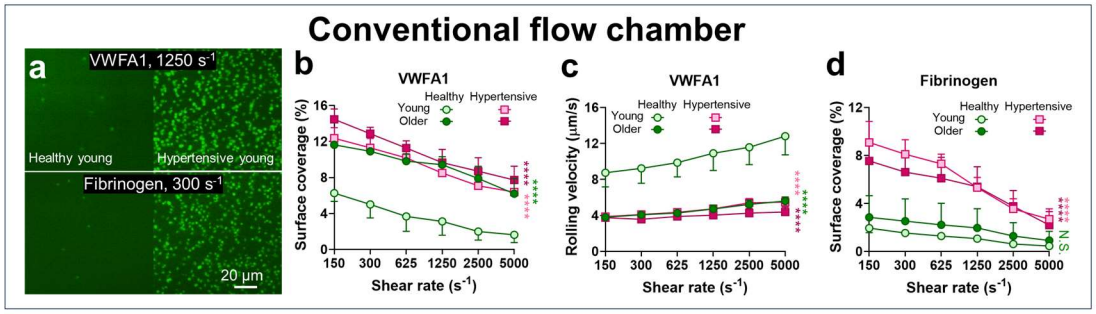
Conventional flow chamber
a
VWFA1, 1250 s-1
Healthy young
Hypertensive young
Fibrinogen, 300 s-1
20 μm
b
VWFA1
Healthy Hypertensive
Young
Older
Surface coverage (%)
Shear rate (s-1)
c
VWFA1
Rolling velocity (μm/s)
Shear rate (s-1)
d
Fibrinogen
Surface coverage (%)
Shear rate (s-1)
N.S.

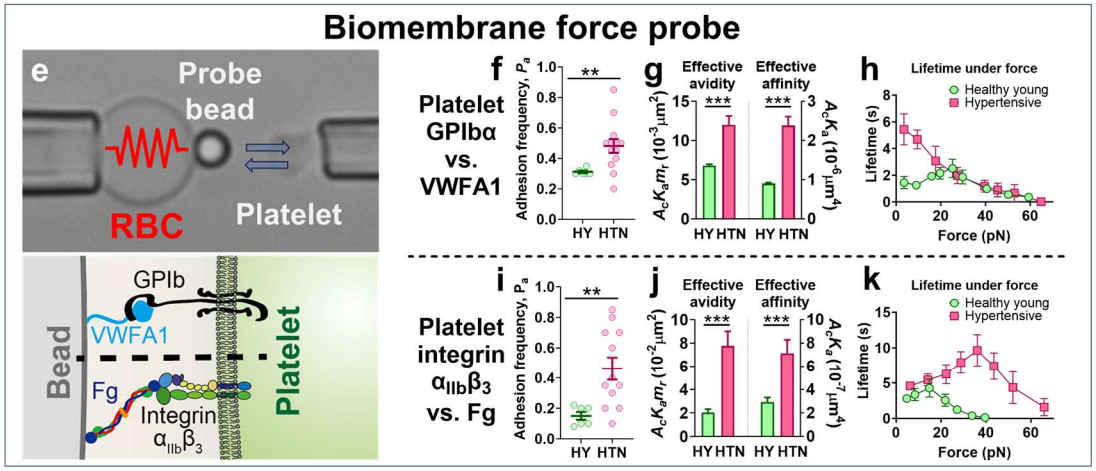
Biomembrane force probe
e
Probe bead
RBC
Platelet
GPIb
VWFA1
Bead
Platelet
Fg
Integrin αIIbβ3
f
Platelet GPIbα vs. VWFA1
Adhesion frequency, Pa
HY HTN
g
Effective avidity
Effective affinity
HY HTN HY HTN
h
Lifetime under force
Healthy young
Hypertensive
Lifetime (s)
Force (pN)
i
Platelet integrin αIIbβ3 vs. Fg
Adhesion frequency, Pa
HY HTN
j
Effective avidity
Effective affinity
HY HTN HY HTN
k
Lifetime under force
Healthy young
Hypertensive
Lifetime (s)
Force (pN)

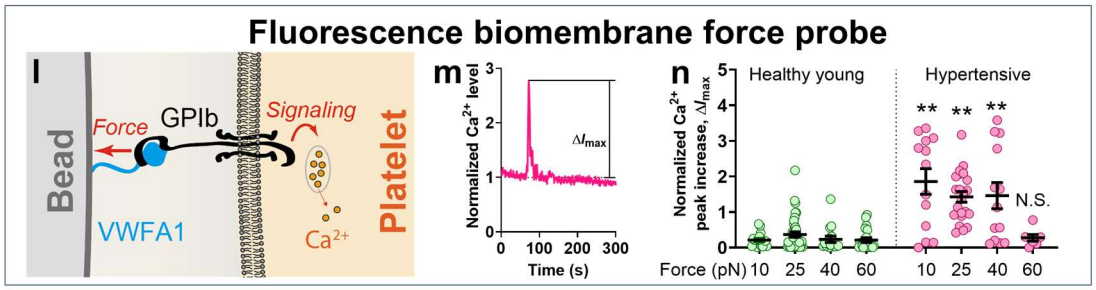
Fluorescence biomembrane force probe
l
Bead
Force
GPIb
Signaling
Platelet
VWFA1
Ca2+
m
Normalized Ca2+ level
ΔImax
Time (s)
n
Normalized Ca2+ peak increase, ΔImax
Healthy young
Hypertensive
N.S.
Force (pN) 10 25 40 60 10 25 40 60

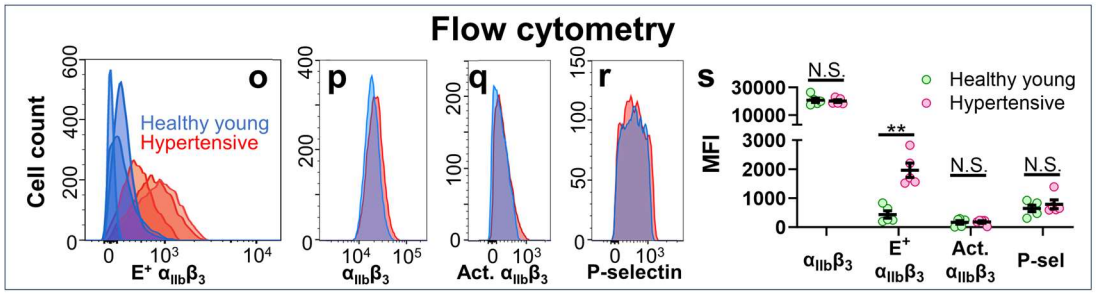
Flow cytometry
Cell count
o
Healthy young
Hypertensive
E+ αIIbβ3
p
αIIbβ3
q
Act. αIIbβ3
r
P-selectin
s
MFI
N.S.
Healthy young
Hypertensive
αIIbβ3
E+ αIIbβ3
Act. αIIbβ3
P-sel

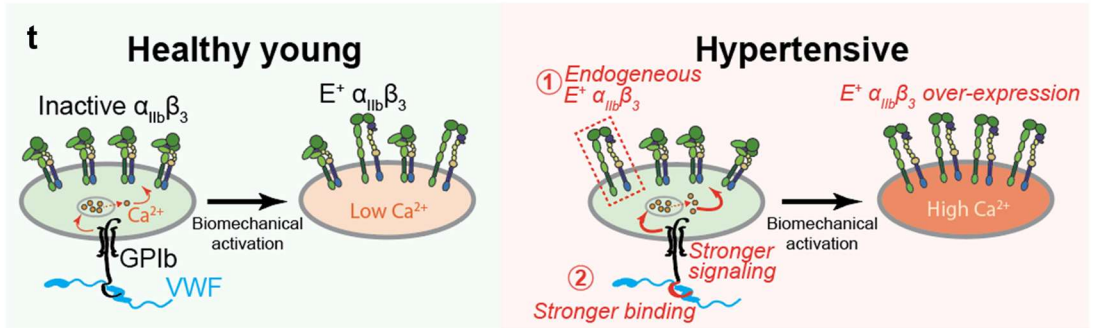
t
Healthy young
Inactive αIIbβ3
E+ αIIbβ3
Ca2+
Biomechanical activation
Low Ca2+
GPIb
VWF
Hypertensive
① Endogeneous E+ αIIbβ3
E+ αIIbβ3 over-expression
Biomechanical activation
High Ca2+
Stronger signaling
②
Stronger binding

Figure 5. Hyperactivity of GPIbα and integrin $\alpha_{IIb}\beta_3$ associated with hypertension. (**a**) Snapshots of healthy young and hypertensive young subjects' platelets adhering to VWFA1 (*upper*) or Fg (*lower*) in flow chamber. (**b-d**) Mean±s.e.m. (n =3) of surface coverage (b,d) and rolling velocity (c) *vs.* shear rate of platelets perfused over a surface pre-coated with 25 μg mL^{-1} VWFA1 (b,c) or 100 μg mL^{-1} Fg for 1 h (d). ****p <0.0001; N.S., not significant, assessed by two-way ANOVA. (**e**) BFP setup photomicrograph (*top*) and molecular binding illustration (*bottom*). (**f-k**) Adhesion frequency (Scatter plots with mean±s.e.m.) (f,i), effective avidity and affinity (Mean±s.e.m.) (g,j) and bond lifetime vs. force (mean±s.e.m., n ≥300 for each curve) (h,k) of VWFA1- (f-h) or Fg- (i-k) coated beads binding to healthy young or hypertensive subjects' platelets. **p <0.01; ***p <0.001, assessed by t-test. (**l**) Illustration of fBFP setup. VWFA1 pulling on GPIbα triggers intraplatelet Ca^{2+} flux. (**m**) Representative time course of a hypertensive subjects' platelet's normalized Ca^{2+} level during repeated VWFA1 pulling at 40-pN clamping force. Peak increase ΔI_{max} is marked. (**n**) Intraplatelet Ca^{2+} peak increase (scatter plot with mean±s.e.m.) of healthy young (*left*) and hypertensive (*right*) subjects' platelets during VWFA1 pulling at different clamping forces. **p <0.01, comparing healthy young and hypertensive at the same forces, assessed by two-way ANOVA. (**o-r**) Representative flow cytometry histograms of E^+ $\alpha_{IIb}\beta_3$ (o; n =3), total $\alpha_{IIb}\beta_3$ (p), Act. $\alpha_{IIb}\beta_3$ (q) and P-selectin (r) signals on healthy young (*blue*) and hypertensive (*red*) subjects' platelets. (**s**) Scatter plot with mean±s.e.m. (n =5) of flow cytometry MFI of total $\alpha_{IIb}\beta_3$, E^+ $\alpha_{IIb}\beta_3$, Act. $\alpha_{IIb}\beta_3$ and P-selectin signals on healthy young (*blue*) and hypertensive (*red*) subject's platelets. **p <0.01; N.S., not significant, assessed by multiple t-test. (**t**) Proposed mechanism model of E^+ $\alpha_{IIb}\beta_3$ over-expression in the biomechanical thrombi of hypertension patients.

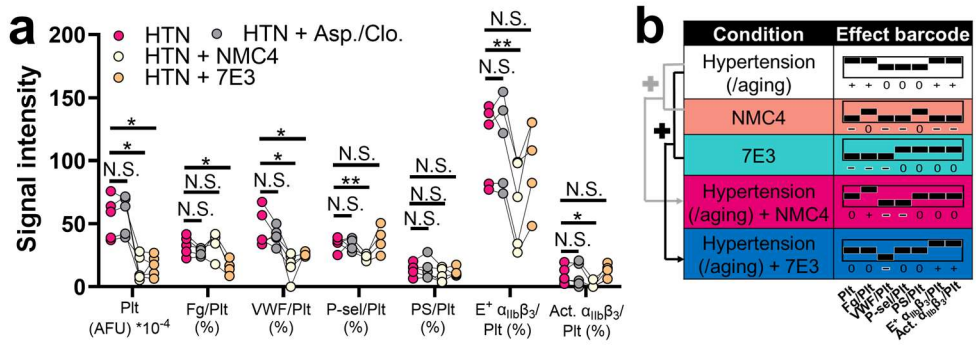
a
HTN
HTN + Asp./Clo.
HTN + NMC4
HTN + 7E3
Signal intensity
200
150
100
50
0
Plt (AFU) *10-4
Fg/Plt (%)
VWF/Plt (%)
P-sel/Plt (%)
PS/Plt (%)
E+ αIIbβ3/ Plt (%)
Act. αIIbβ3/ Plt (%)
N.S.
*
**
b
Condition
Effect barcode
Hypertension (/aging)
NMC4
7E3
Hypertension (/aging) + NMC4
Hypertension (/aging) + 7E3
Plt
Fg/Plt
VWF/Plt
P-sel/Plt
PS/Plt
E+ αIIbβ3/Plt
Act. αIIbβ3/Plt

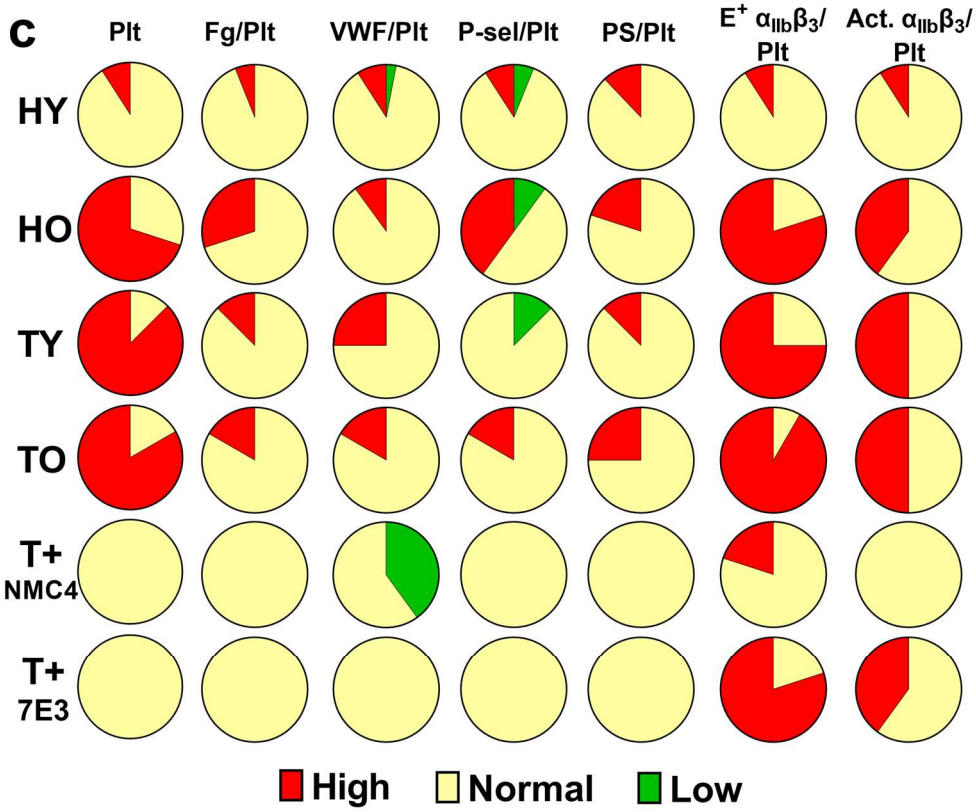
c
Plt
Fg/Plt
VWF/Plt
P-sel/Plt
PS/Plt
E+ αIIbβ3/ Plt
Act. αIIbβ3/ Plt
HY
HO
TY
TO
T+ NMC4
T+ 7E3
High
Normal
Low

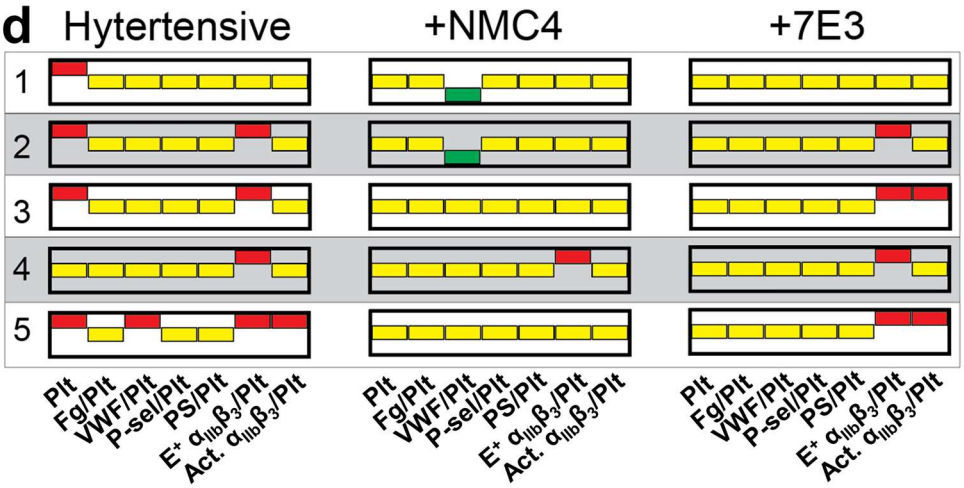
d
Hytertensive
+NMC4
+7E3
1
2
3
4
5
Plt
Fg/Plt
VWF/Plt
P-sel/Plt
PS/Plt
E+ αIIbβ3/Plt
Act. αIIbβ3/Plt

Figure 6. Drug-disease interactions and personal thrombus barcodes. (**a**) Individual point plot (n =5; lines connecting points of the same subjects) of the thrombus profiles of hypertension patients without and with aspirin/clopidogrel (2×), NMC4 (IC50) and 7E3 (IC50) treatment. N.S., not significant; *p <0.05; **p <0.01, assessed by two-way ANOVA. (**b**) The 7-digit effect barcodes of hypertension without and with NMC4 or 7E3 treatment. A rule of addition is indicated. (**c**) Fractions of abnormally high, normal and abnormally low values in each dimension of the personal thrombus barcodes from healthy young (HY), healthy older (HO), hypertensive young (TY), hypertensive older (TO), hypertensive (T)+NMC4 and hypertensive (T)+7E3 groups. (**d**) Comparing the personal thrombus barcodes of hypertensive subjects without and with NMC4 or 7E3 inhibition. Blood samples from a total of 5 subjects was tested. For easier visualization, bars indicating 'high', 'normal' and 'low' are respectively marked by red, yellow, and green.